

# STRUCTURE AND DYNAMICS OF BRANCHED (EPOXY) POLYMERS AND KINETICS OF ITS POLYMERIZATION PROCESS

by

Benjamin Chu and Chi Wu  
Department of Chemistry  
State University of New York at Stony Brook  
Long Island, New York 11794-3400  
U. S. A.

ABSTRACT. Laser light scattering (LLS) and small-angle x-ray scattering (SAXS) studies have been made of the curing of epoxy resins from 1,4-butanediol diglycidyl ether with cis-1,2-cyclohexanedicarboxylic anhydride. The epoxy resin before its gelation threshold is soluble in methyl ethyl ketone, and scattering techniques can be used to determine the weight-average molecular weight ( $M_w$ ), the fractal dimension ( $d_f$ ), and the molecular weight distribution (MWD) of the branched epoxy polymer during each stage of the initial polymerization process. The MWDs obtained from LLS were compared with those determined by conventional size exclusion chromatography (SEC). From the comparison, we were able to develop a new absolute calibration procedure for SEC of specific branched polymers. By investigating the LLS envelope of the three-dimensional crosslinking process near and pass the gelation threshold and by applying the Debye-Bueche theory of light scattering for inhomogeneous solids, the structural changes of the branched epoxy polymer during the curing process could be evaluated. The change in the correlation length ( $a$ ) and the mean squared average of local dielectric constant fluctuations ( $\eta^2$ ) could be divided into four main stages. Finally, The branching kinetics of the copolymerization reaction could be approximated by using Smoluchowski's coagulation equation.

## 1. INTRODUCTION

The kinetics and mechanism of copolymerization of epoxy resins with anhydrides, with or without a catalyst, have been of interest because these materials often constitute an important component in reinforced composites. However, the mechanism of the curing reaction of epoxy resins and anhydrides has been somewhat uncertain as a number of partially conflicting reaction mechanisms have been proposed in recent years<sup>1</sup>. With our light and x-ray scattering techniques, we find that our data, obtained from the curing of 1,4-butanediol diglycidyl ether with

cis-1,2-cyclohexane-dicarboxylic anhydride, in the presence of benzyl dimethyl amine as a catalyst, can best be fitted by the zeroth-order reaction. However, it is not crucial for us to know how the reaction is initiated if we focus our attention mainly to the branching kinetics, and the structure and dynamics of branched epoxy polymer products during different stages of the copolymerization reaction process.

In this article, we shall review four aspects of our studies: (i) the branching kinetics of the copolymerization reaction based on Smoluchowski's coagulation equation, (ii) the concept of fractal geometry as applied to epoxy structures, (iii) the determination of molecular weight distribution of branched epoxy polymers based on Brownian dynamics and (iv) the characterization of structural inhomogeneities based on the Debye-Bueche theory.

(i) the branching kinetics of the copolymerization reaction and the distribution of highly branched epoxy copolymers can be approximated by Smoluchowski's coagulation equation. The equation has been applied to study the structure of clusters produced by the kinetic aggregation of colloidal particles.<sup>2-11</sup> If we take the overall branching probability  $w(i,j)$  to be proportional to the sum of active sites on the two polymers, i.e.  $w(i,j) \propto (i+j)$  where  $i$  and  $j$  are the active sites on polymers  $i$  and  $j$ , respectively, the kinetic equation can be solved explicitly to obtain the weight-average molecular weight ( $M_w$ ) and the molecular weight distribution (MWD) at different reaction stages.

(ii) The concept of fractal geometry<sup>12,13</sup> can be applied to investigations cured epoxy systems. The fractal concept has shown to be a useful approach to describe the structure of random systems, such as aggregates of colloidal silica,<sup>14-16</sup> branched silica condensation polymers,<sup>17</sup> cross-linked poly(dimethyl -siloxane),<sup>18,19</sup> aggregating proteins<sup>20</sup> and gold colloids,<sup>21</sup> as well as diffusion-limited<sup>22,23</sup> polymerization of the conducting polymer polypyrrole<sup>24</sup> and other growth processes, e.g., percolation<sup>25</sup> and cluster-cluster aggregation.<sup>26-28</sup>

(iii) the molecular weight distribution (MWD) of the branched epoxy polymer formed during each reaction stage can be estimated by means of dynamic light scattering. The procedure is as follows. Estimates of the normalized characteristic line-width ( $\Gamma$ ) distribution function,  $G(\Gamma)$ , can be obtained from the measured intensity-intensity time correlation function,  $G^{(2)}(\tau)$ , by using the Laplace inversion.  $G(\Gamma)$  can then be transformed to the molecular weight distribution by incorporating information based on the static and dynamic properties of the branched epoxy polymer solution, i.e. the weight-average molecular weight ( $M_w$ ), the second virial coefficient ( $A_2$ ), the z-average root-mean-square radius of gyration ( $R_g$ ), the diffusion second virial coefficient ( $k_d$ ), the z-average translational diffusion coefficient at infinite dilution

$(\bar{D}_0^0)$ , and the scaling relation  $D_0^0 = k_D M^{-\alpha_D}$ . Knowledge gained from laser light scattering (LLS) of our broad MWD epoxy polymers is sufficient to calibrate the size exclusion chromatographic (SEC) column for specific branched epoxy polymer studies.

(iv) The laser light scattering intensity envelope in the presence of different amounts of catalyst at different temperatures (60, 70, 80 and 90°C) can be analyzed according to the Debye-Bueche theory.<sup>29</sup> The intensity of light scattered by an inhomogeneous medium is dependent upon the local refractive index difference in the inhomogeneous medium in terms of the mean square average of local dielectric constant fluctuations  $\bar{\eta}^2$  which can be related to structural changes during the copolymerization process.

Experimentally, we used small angle x-ray scattering (SAXS) at the State University of New York (SUNY) X21A2 beamline, National Synchrotron Light Source (NSLS), Brookhaven National Laboratory (BNL) and laser light scattering (LLS) to measure the angular distribution of absolute scattered intensity  $I(\theta)$  and  $G^{(2)}(r)$  at different reaction stages with % conversion determined by chemical analysis. From  $I(\theta)$  in dilute solution, we can determine  $M_w$ ,  $R_g$ ,  $A_2$  and the fractal dimension ( $d_f$ ).

By using the Laplace inversion, we can transform  $G^{(2)}(r)$  to estimate  $G(\Gamma)$  which can be used to estimate the molecular weight distribution. The experimental results are then compared with the calculated values based on an analytical solution of Smoluchowski's coagulation equation, using the simplest reasonable assumption concerning the functional form of the reaction kernel in that equation. The comparison indicates that the equation provides a useful theoretical framework for the interpretation of the experimental results but requires a kernel of more general form in order to be of value in making quantitative predictions. From  $I(\theta)$  measured in situ during the curing process, the correlation length ( $a$ ) which characterizes the extension of the local inhomogeneous domain and the mean square average dielectric constant fluctuations ( $\bar{\eta}^2$ ) could be used to characterize the changes in optical inhomogeneities at different copolymerization stages. The changes can be divided into four main stages as the reaction progresses.

## 2. EXPERIMENTAL METHODS

### 2.1 Materials.

1,4-butanediol diglycidyl ether (DGEB,  $M_w = 202.3$  g/mol) and cis-1,2-cyclohexanedicarboxylic anhydride (CH,  $M_w = 154.2$  g/mol) were purchased from Aldrich Chemical Company and used without further purification

since we were able to obtain the same experimental results after both components were purified by vacuum ( $\approx 0.01$  mm Hg) distillation. The catalyst (CA), benzyl dimethyl amine ( $M_w = 135.2$  g/mol), courtesy of Gary L. Hagnauer, Polymer Research Division, Army Materials Technology Laboratory, Watertown, Mass.) was vacuum distilled before use.

## 2.2 Preparation of Solutions.

Known weights of CH were heated to  $\sim 50^\circ\text{C}$  in order to melt the CH. The melted CH was then cooled to  $\sim 37^\circ\text{C}$ , a few degrees above the melting point of CH ( $\sim 32\text{--}34^\circ\text{C}$ ), and mixed well with known weights of DGEb. Then, a small amount of catalyst was added to the homogeneous liquid mixture using a Drummond digital microdispenser ( $\pm 0.01$   $\mu\text{L}$ ). The well-mixed reaction mixture containing a molar ratio of epoxy (DGEb) : curing agent (CH) : catalyst (CA) = 1:2:0.001 was reacted at  $80^\circ\text{C} \pm 0.5^\circ\text{C}$  in an oil bath. Samples containing the epoxy polymer and unreacted monomers (DGEb and CH) were withdrawn from the reaction mixture during the course of the copolymerization reaction until the gel point was reached. Compositions of the reaction mixture could be analyzed chemically.<sup>30</sup> Portions of withdrawn samples were further dissolved in methyl ethyl ketone (MEK) for LLS measurements and in tetrahydrofuran (THF) for SEC measurements. Concentrations of the epoxy polymer ranged from  $\sim 1 \times 10^{-3}$  g/mL for LLS experiments to  $\sim 1 \times 10^{-2}$  g/mL for SEC experiments. Samples for LLS measurements were centrifuged at 7000 gravity and room temperatures for four hours. A middle portion of the centrifuged solution was then transferred to dust-free cylindrical light scattering cells of 10-17 mm o.d. by using a dust-free pipet.

## 2.3 Methods of Measurement.

A high-temperature light-scattering spectrometer was used for measurements of the angular distribution of absolute scattered intensity as well as its spectral distribution.<sup>31</sup> The glass jacket (4 in Figure 2 of ref 31) was modified so that the inner brass thermostat (5 in Figure 2 of ref 31) was immersed in a glass jacket containing refractive-index matching oil. This more standard arrangement permitted a reduction in the o.d. of the cylindrical light-scattering cell to between 10 and 17 mm and consequent reduction in the solution volume required to carry out light-scattering experiments. With the refractive index matching oil, we could also cover a broader scattering angular range varying from about  $10^\circ$  to  $140^\circ$ , even though the smaller accessible scattering angular range was relatively unimportant for the epoxy characterization, especially during the initial curing process. The details of laser light-scattering instrumentation have been described elsewhere.<sup>31</sup>

We have modified a Kratky block collimation system<sup>32</sup> for SAXS at SUNY X21A2 beamline, NSLS, BNL. For the epoxy polymer studies, we used a slit width of  $\sim 0.5$  mm and covered a  $K$  range between  $\sim 0.07$  and  $3.4 \text{ nm}^{-1}$  where the scattering wave vector  $K = (4\pi/\lambda)\sin(\theta/2)$  with  $\lambda$  and  $\theta$  being an X-ray wavelength of  $0.154 \text{ nm}$  and the scattering angle, respectively. Two ionization chambers were used to measure the sample transmission and reference intensity. The SAXS curves were corrected for detector linearity, parasitic scattering, solvent background, and sample attenuation. Desmearing was unnecessary as the incident X-ray beam had a small cross section of  $0.5 \times 2 \text{ mm}$  at the sample chamber.

For SEC experiments, we used three ultrastyrigel columns designated as  $10^2 \text{ \AA}$ ,  $10^3 \text{ \AA}$  and  $10^4 \text{ \AA}$  (Waters Associates) connected in series, a pump (Waters Model 590) operating at a flow rate of  $1.0 \text{ mL/min}$ , and a differential refractometer (Waters Model R401) as the detector. The chromatogram was simultaneously recorded on a strip chart recorder and a microcomputer. The sample injection volume was  $50 \mu\text{L}$  with a concentration of  $\approx 1 \times 10^{-2} \text{ g/mL}$ , which is below the over-loading condition. All SEC experiments were performed at  $45^\circ\text{C}$  in order to increase the efficiency of the columns.

### 3. Results and Discussion.

#### 3.1. Refractive Index Increment Measurements.

An absolute determination of the polymer molecular weight requires information on the refractive index increment  $(\partial n/\partial C)_{T,P} \approx dn/dC$  as well as the Rayleigh ratio. The refractive index increment was determined according to the procedure outlined in reference 31. We did not try to isolate the epoxy polymer from varying amounts of unpolymerized DGEb and CH. Instead, we determined  $dn/dC$  for the epoxy polymers in MEK in the presence of small amounts of DGEb and CH.

We have taken into account the varying amounts of DGEb and CH by adding corresponding quantities of unreacted DGEb and CH with the solvent MEK in order to keep the ratio of MEK:DGEb:CH constant for the branched epoxy polymer solutions. Thus, for each branched epoxy polymer which we withdrew from the reaction mixture, we dissolved the polymer at different concentrations using a mixed solvent with a constant ratio of MEK:DGEb:CH. Furthermore, we took into account possible solvent preferential interactions by using two different mixed solvent ratios (MEK:DGEb:CH =  $1:0.03:0.025$  and  $1:0.001:0.007$  in volume ratios). The same results (molecular weight and radius of gyration) were obtained. Thus, we do not have to take into account the small variation in the mixed solvent composition in our analysis.  $dn/dC = 0.180 \pm 0.002$  within the above two volume ratios of MEK:DGEb:CH at  $\lambda_0 = 488 \text{ nm}$  and  $25^\circ\text{C}$  and the refractive index of the corresponding solvent mixture is  $1.377$ .

### 3.2. Light Scattering Intensity Measurements.

The excess absolute integrated intensity of light scattered by a dilute polymer solution has the form

$$\frac{HC}{R_{vv}(K)} = \frac{1}{M_w} \left( 1 + \frac{K^2 R_g^2}{3} \right) + 2A_2 C \quad (1)$$

where the optical constant  $H = (4\pi^2 n^2 / N_A \lambda_o^4) (dn/dc)^2$ , with  $\lambda (= \lambda_o/n)$ ,  $A_2$ ,  $R_g^2 (= \langle R_g^2 \rangle_z^{1/2})$ ,  $M_w$  and  $K$  being, respectively, the wavelength of light in the scattering medium, the second virial coefficient, the z-average root-mean-square radius of gyration, the weight average molecular weight and the magnitude of the momentum transfer vector. The subscripts vv denote vertically polarized incident and scattered light. From a Zimm plot as shown typically in Figure 1, we can determine  $M_w$ ,  $R_g$  and  $A_2$ . The results are listed in Table I.

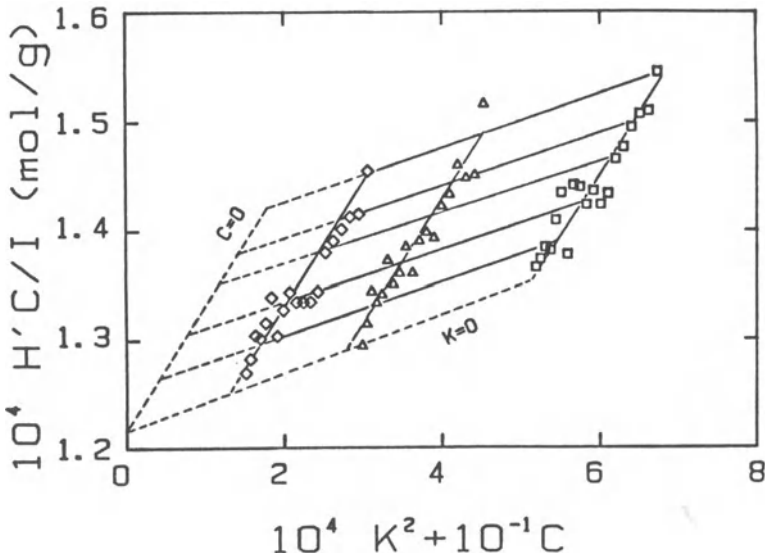


Figure 1. Typical Zimm plot of epoxy polymer in methyl ethyl ketone with traces of unreacted monomers DGEb and CH at 25°C using light scattering intensity measurements with  $\lambda_o = 488$  nm sample 12 with ~45.3% CH conversion.  $M_w = 3.01 \times 10^5$  g/mol,  $A_2 = 2.88 \times 10^{-4}$  mL mol g<sup>-2</sup>,  $R_g = 25.7$  nm: ( $\Delta$ )  $C = 1.17 \times 10^{-4}$  g/mL; ( $\square$ )

$C = 4.27 \times 10^{-4}$  g/mL; ( $\diamond$ )  $C = 7.54 \times 10^{-4}$  g/mL. (Reproduction of Fig. 1 of Ref. 77)

### 3.3. Small Angle X-Ray Scattering Measurements.

In SAXS, the excess scattered intensity  $I$  is governed by electron density (instead of refractive index) differences between the solute and the solvent. We may write

$$\frac{H'C}{I} = \frac{1}{M_w} \left( 1 + \frac{K^2 R_g^2}{3} \right) + 2A_2 C \quad (2)$$

where the optical constant  $H$  in light scattering has been replaced by an instrument constant  $H'$  which takes care of the square effect due to the electron density increment<sup>33</sup> and instrumentation differences between light scattering and SAXS. Without computing or measuring the electron density increment, we simply determined  $H'$  by using an epoxy polymer (sample 3) of known molecular weight ( $8.23 \times 10^3$  g/mol from light scattering measurements) as our SAXS calibration standard. SAXS intensity measurements could then be used to determine  $M_w$ ,  $R_g$  and  $A_2$  of other epoxy polymer samples (1,2,4-7) as shown typically in Figure 2.

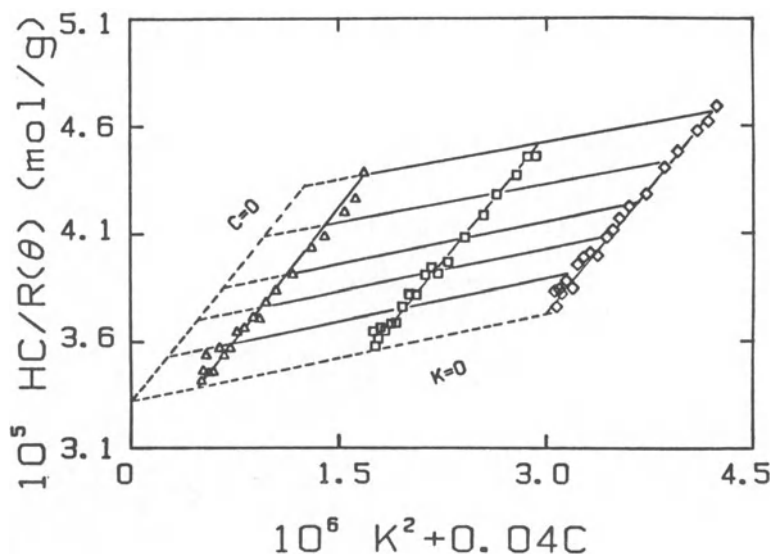


Figure 2. Typical Zimm plot of epoxy polymer in methyl ethyl ketone with traces or unreacted monomers DGEb and CH at 25°C using small angle x-ray scattering at the National Synchrotron Light

Source  $\lambda = 0.154$  nm. Sample 3 with  $\sim 20\%$  conversion.  $M_w = 8.23 \times 10^3$  g/mol,  $A_2 = 1.05 \times 10^{-3}$  mL mol g $^{-2}$ ,  $R_g = 4.4$  nm: ( $\diamond$ )  $C = 7.89 \times 10^{-4}$  g/mL; ( $\Delta$ )  $C = 1.04 \times 10^{-3}$  g/mL; ( $\square$ )  $C = 2.51 \times 10^{-3}$  g/mL. H'C/I transfers the light scattering calibration to SAXS by determining the ratio of scattering intensities in light scattering and SAXS of one epoxy polymer solution of known molecular weight. (Reproduction of Fig. 2 of Ref. 77)

The SAXS results are also listed in Table I. The agreement between light scattering and SAXS results is very good, with  $M_w$  values differing by no more than a few percent in most cases. From the initial slopes in plots of  $\lim_{C \rightarrow 0} HC/R_{VV}$  and  $\lim_{C \rightarrow 0} H'C/I$  versus  $K^2$ , we note that for sample 7,  $R_g = 112\text{\AA}$  and  $105\text{\AA}$  by means of SAXS and light scattering, respectively. An  $R_g$  value of  $\sim 100\text{\AA}$ , as determined by light scattering, has an uncertainty of about 10%, while SAXS with the intense synchrotron x-ray source yields fairly precise  $R_g$  values with uncertainties of no more than a few percent down to very small sizes (e.g.  $R_g$  (sample 1) =  $29\text{\AA}$ ).

In Figure 2, the unsmoothed excess SAXS intensity has been corrected for detector nonlinearity, sample transmission, solvent background and parasitic scattering. No desmearing was required because of the small beam cross section and divergence of the incident synchrotron x-ray beam. The agreement of  $R_g$  values between light scattering and SAXS also confirms the above assumption over the  $K$  range of our measurements. It should also be noted that the signal-to-noise ratio of our SAXS measurements is better than Figure 2 suggests, as the intensity values have been greatly magnified in order to show the initial slope behavior from the first 19 data points at the lowest scattering angles. If we were to use a conventional x-ray source, we would have great difficulty in achieving such a reciprocal intensity plot. Rather, a Guinier plot of  $\log I$  versus  $K^2$ , as shown in Figure 3, represents the standard method of determining  $R_g$ . According to Eq. (2), we have for  $C=0$

$$\log(I/H'C) \approx \log M_w + \log\left(1 - \frac{K^2 R_g^2}{3}\right) \approx \log M_w - \frac{K^2 R_g^2}{3} \quad (3)$$

The limiting slope at  $C=0$  and  $KR_g \ll 1$  yields the radius of gyration. The linear behavior over a much broader  $K$ -range in SAXS permits a more precise  $R_g$  determination for small  $R_g$  values ( $\leq 100\text{\AA}$ ) by means of SAXS when compared with light scattering. In polymer characterization, light

scattering and SAXS are truly complementary techniques in covering the size determination.

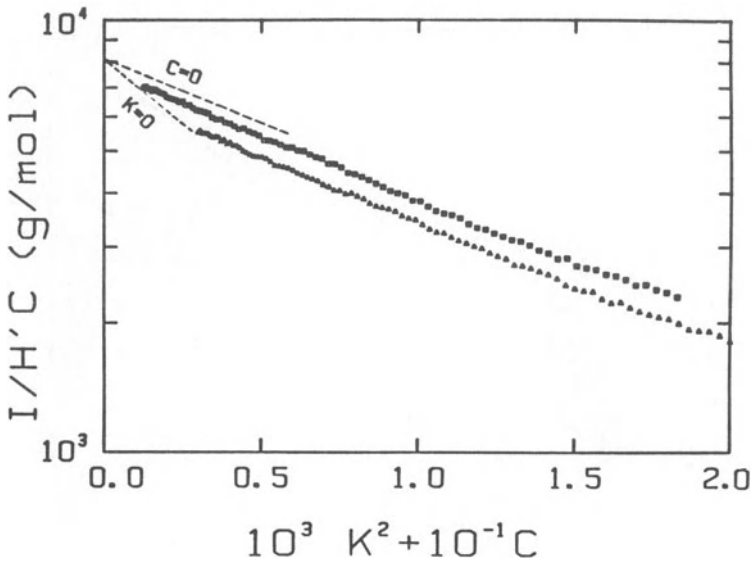


Figure 3. Guinier plots of two of the three concentrations of Fig. 2 ( $\square$ )  $C = 7.89 \times 10^{-4}$  g/mL; ( $\triangle$ )  $C = 2.51 \times 10^{-3}$  g/mL. From the initial slopes, we retrieved essentially the same values for  $M_w$ ,  $A_2$  and  $R_g$  as stated in Fig. 2. The linear behavior in a  $\log I$  versus  $K^2$  plot at  $KR_g < 1$  in the SAXS measurements is clearly demonstrated. (Reproduction of Fig. 3 of Ref. 77)

For our epoxy studies, we started with monomers which eventually form very large polymer networks. Thus, during the initial stages of the epoxy polymerization process, SAXS is the proper analytical method to determine  $R_g$  of the branched epoxy polymer. Following Eqs. (1) and (3)

$$\lim_{C \rightarrow 0} \frac{M_w HC}{R_{vv}(K)} = \lim_{C \rightarrow 0} \frac{M_w H' C}{I(K)} = 1 + (R_g/3)K^2 R_g = 1 + (R_g/3)\chi \quad (4)$$

In plots of  $\lim_{C \rightarrow 0} M_w HC/R(\theta)$  or  $\lim_{C \rightarrow 0} M_w H' C/I$  versus  $\chi (=K^2 R_g^2)$ , as shown in Figure 4, we see that LLS measurements, as denoted by filled symbols are clearly appropriate for  $R_g$  values of a few hundred Å. It becomes increasingly more difficult at smaller  $R_g$  values because of the small  $KR_g (< 1)$  ranges accessible to LLS. For sample 7 (denoted by filled and

hollow diamonds) we demonstrate an overlap of two independent scattering techniques on an absolute determination of  $R_g$ .

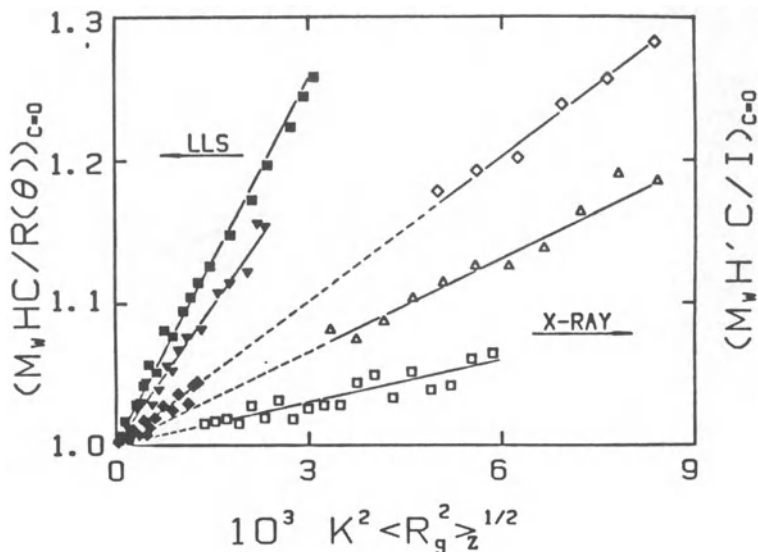


Figure 4. Plots of  $M_w HC/R_{vv}$  (for light scattering) and  $M_w H' C/I$  (for SAXS) as a function of  $K^2 \langle R_g^2 \rangle^{1/2}$ . According to Eqs. 1 and 3,

$$\lim_{C \rightarrow 0} \frac{M_w HC}{R_{vv}} (= \lim_{C \rightarrow 0} \frac{M_w H' C}{I}) = 1 + \frac{R_g}{3} K^2 \langle R_g^2 \rangle^{1/2}. \quad \text{Thus, the}$$

slope is equal to  $R_g/3$ . The plots demonstrate overlapping regions of the two scattering techniques. Laser light scattering is denoted by filled symbols while SAXS is denoted by hollow symbols. (■) Sample 12, (▼) sample 10, (◆) sample 7; (◇) sample 7, (△) sample 5, (□) sample 3. Properties of various samples are listed in Table I. (Reproduction of Fig. 4 of Ref. 77)

### 3.4. Fractal Geometry of Branched Epoxy Polymers

The curing of epoxy resins using DGEBA and CH in the presence of a small amount of catalyst CA represents a cross-linking polymerization process, as shown schematically in Figure 5. The cross linking reaction involves roughly  $n$  moles of DGEBA with  $2n$  moles of CH. The chemical reaction is known to cluster at catalytic centers and the formation of branched structures eventually link together the branched epoxy polymers to form loops or polymer networks.

The concept of fractal geometry<sup>12,34,35</sup> can be a useful tool to

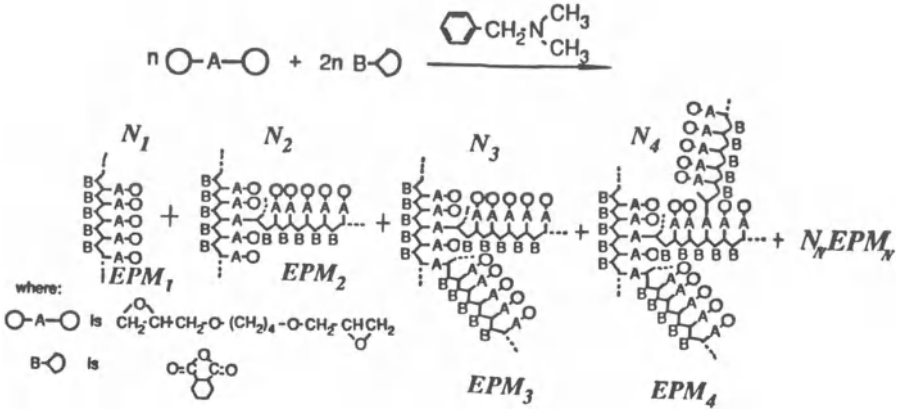


Figure 5. Crosslinking reaction of DGEBA with CH in the presence of CA. (Reproduction of Fig. 1 of Ref. 79)

describe the branching structure of epoxy polymers during its curing process. The fractal dimension  $d_R$  of a molecular cluster with mass  $M$

and the radius of gyration has the relation<sup>36</sup>  $M \sim R_g^{d_R}$  where  $d_R$  is the fractal dimension in terms of the scaling relationship between mass and radius of gyration. For polydisperse polymers, we approximate the expression to be

$$M_w \sim R_g^{d_R} \tag{5}$$

In Eq. (5), we have assumed that  $M_w$  spacings have been sufficiently far apart so that the polydispersity effect is not appreciable. It should be noted that polydispersity could act as a simple correction<sup>37</sup> or could affect the measured exponents  $d_R$ <sup>38-40</sup> as well as  $d_K$ .<sup>41,42</sup> The two-point density-density correlation function  $C(r)$  has the form<sup>22</sup>  $C(r) \approx C_0 r^{-\alpha}$  with the corresponding static structure factor  $S(K)$  ( $\sim$  the scattered intensity  $I$ ), which is the Fourier transform of the pair correlation function, having a power-law relation

$$S(K) \sim K^{-d_K} \tag{6}$$

The fractal dimension  $d_K$  is related to the exponent  $\alpha$  according to  $d_K = d - \alpha$  with  $d$  being the dimensionality of the embedding space or lattice containing the fractal. For a self-similar fractal  $d_f = d_K = d_R$  where  $d_f$  is a general fractal dimension.<sup>43</sup> Measurements of the angular distribution of scattered intensity over large ranges of  $K$  with  $R_g^{-1} < K < \xi^{-1}$  permit us to determine  $d_K$  according to Eq. (6) where  $\xi$  is a correlation length related to the "blob" size. Measurements of  $M_w$  and  $R_g$  of the epoxy polymer by means of Zimm plots during the polymerization process permit us to determine  $d_R$  according to Eq. (5). In this section, our main aim is to check Eqs. (5) and (6) and to find out if our epoxy polymers form self-similar fractals.

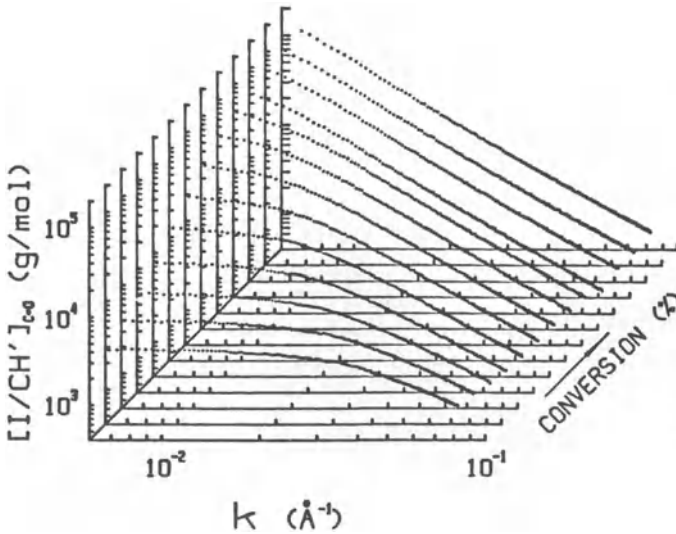


Figure 6. Structure of epoxy polymers as a function % CH conversion.  $[I/CH']_{C=0}$  represents absolute SAXS intensity at infinite dilution in units of g/mol. Thus,  $\lim_{K \rightarrow 0} [I/CH']_{C=0} = 1/M_w$ . The scattering curves are numbered with increasing % CH conversion. Properties of the 13 samples representing epoxy polymers during different stages of the curing process are listed in Table I. (Reproduction of Fig. 6 of Ref. 77)

Figure 6 shows static structure factors  $S(K)[= I/CH']$  from SAXS as a function of % CH conversion. In plotting the scattering curves, we have scaled the intensities according to Eq. (3). Thus, the  $y(= \lim_{C \rightarrow 0} I/CH')$  axis has units of g/mol and at  $K = 0$ , denotes the  $M_w$  of the epoxy polymer as a function of % CH conversion. Such an approach is feasible up to the gelation point, beyond which the epoxy polymer can no longer be dissolved as individual macromolecules in MEK. At high % CH conversion, the epoxy polymer has reached fairly high molecular weights ( $\sim 10^5$  g/mol). Thus, SAXS measures mainly the fractal geometry of the branched epoxy polymers in solution according to Eq. (6), as shown typically in Figure 7 by the hollow diamonds for sample 13 with a  $M_w$  of

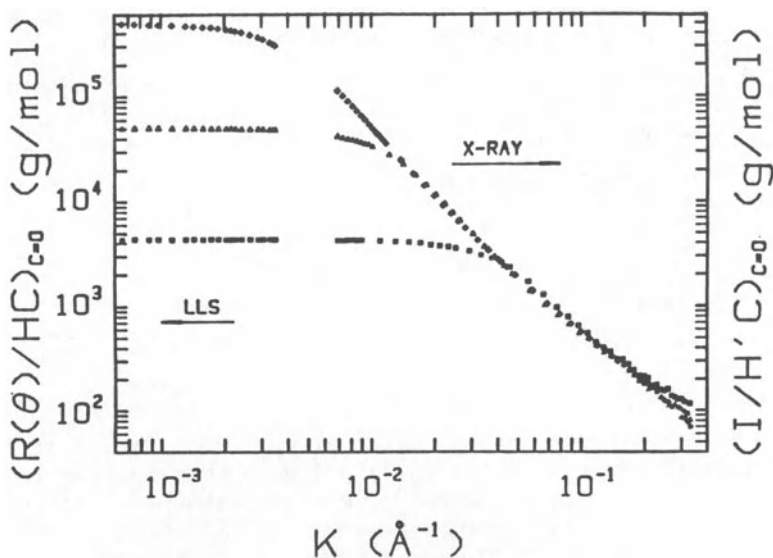


Figure 7. Log-log plots of  $R/HC$  for light scattering and  $I/H'C$  for SAXS as a function of  $K$ . ( $\square$ ) sample 1, ( $\nabla$ ) sample 7, ( $\diamond$ ) sample 13. Light scattering  $K$  range:  $\sim 7 \times 10^{-4} < K < 4 \times 10^{-3} \text{ \AA}^{-1}$ ; SAXS  $K$  range:  $7 \times 10^{-3} < K < 3.5 \times 10^{-1} \text{ \AA}^{-1}$ . Each SAXS curve has 817 data points, of which only a fraction is plotted. The horizontal portion of the scattering curve with a small initial negative slope can be related to the radius of gyration. In the range  $2/R_g < K < 1/20 \text{ \AA}^{-1}$ , we can use the scattering curves to examine fractal geometry of the epoxy polymers. (Reproduction of Fig. 7 of Ref. 77)

$5 \times 10^5$  g/mol. In Figure 7, we have also included LLS measurements (also denoted by hollow diamonds) at much smaller values of  $K (< 4 \times 10^{-3} \text{ \AA}^{-1})$ .

It may be difficult to see from Figure 7 that the initial slope from LLS exhibiting almost horizontal behavior could easily determine the  $R_g$  value as has been demonstrated by Figure 1. As the K-range covered by SAXS is extremely broad, i.e., down to monomer dimensions, we would also expect a deviation from the fractal dimension beyond  $2/R_g \leq K \leq 1/20 \text{ \AA}^{-1}$ , i.e.,  $20K \lesssim 1$  with K expressed in  $\text{\AA}^{-1}$ . Sample 13 represents the epoxy polymer structure just before its gelation point. At earlier times, e.g. for sample 7 with  $M_w = 5 \times 10^4$  g/mol at 38.5% CH conversion, the initial slope from SAXS and that from LLS (both denoted by solid triangles) in Figure 7 could be used to determine  $R_g$ . The log-log plot of Figure 7 also demonstrates the precision with which we have to achieve in order to measure  $R_g$  of the order of  $100 \text{ \AA}$ . The LLS portion of the solid triangles is almost horizontal. We have also included sample 1 (denoted by hollow squares) representing only a 6.5% CH conversion in Figure 7. For sample 1,  $R_g$  ( $\sim 29 \text{ \AA}$ ) is no longer accessible by LLS. In the SAXS region, the initial horizontal curve can be used to determine both  $M_w$  and  $R_g$ . Again, we can use Eq. 6 to determine the fractal dimension over an appropriate K range ( $2/R_g \leq K \leq 1/20 \text{ \AA}^{-1}$ ). More importantly, we note that the scattering curves of samples 7 and 13 overlap over a broad K-range ( $1.5 \times 10^{-2} \leq K \leq 3 \times 10^{-1} \text{ \AA}^{-1}$ ) while the scattering curve for sample 1 with  $M_w = 4 \times 10^3$  g/mol does not overlap with the other two scattering curves even in a log-log plot, indicating structural differences for the epoxy polymer between the very initial stages and before the gelation. We shall return to this point later. In Figure 7, the scattering curves have similar shapes and we want to again emphasize the complementary aspect of the two scattering techniques. For our epoxy polymerization process, we need both LLS and SAXS in order to cover the appropriate K ranges.

Now we turn our attention to the two main tasks, i.e., experimental determinations of  $d_K$  and  $d_R$ . For  $d_K$ , we can determine a value for each sample. However, for  $d_R$ , instead of doing a tedious fractionation of each polymer sample, we have chosen the approximate Eq. (5) and made an experimental determination of  $M_w$  and  $R_g$  for the epoxy polymer at 13 time intervals up to the neighborhood of the gelation threshold during the curing process.

In the  $d_K$  determination, we have considered the concentration effect as follows. Figure 8(a) shows log-log plots of  $I/H'$  versus K for sample 10 in MEK at  $C = (\ ) 7.19 \times 10^{-4}$  g/mL,  $(\Delta) 1.14 \times 10^{-3}$  g/mL, and  $(\square) 2.41 \times 10^{-3}$  g/mL. As we have a total of 817 data points for each

scattering curve, only a fraction of the data is plotted. It should be

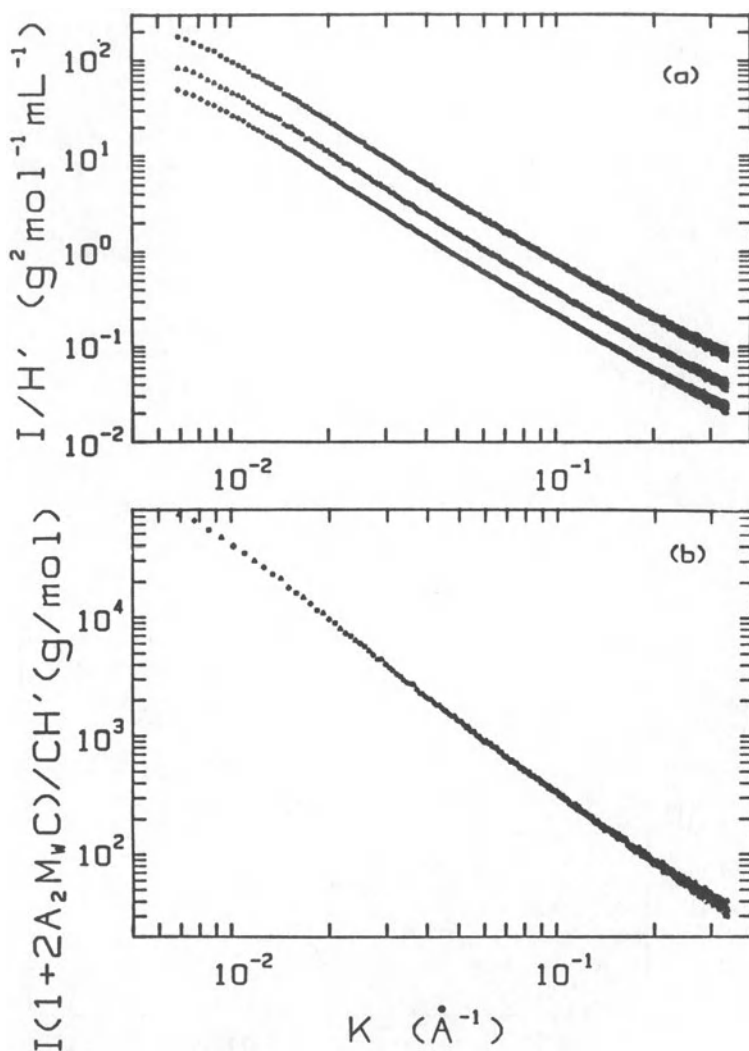


Figure 8. Concentration effect on fractal dimension of epoxy polymers. (a) Log-log plots of  $I/H'$  versus  $K$  for sample 10 in MEK. ( $\diamond$ )  $C = 7.19 \times 10^{-4}$  g/mL; ( $\nabla$ )  $C = 1.14 \times 10^{-3}$  g/mL; ( $\square$ )  $C = 2.41 \times 10^{-3}$  g/mL. There are 817 data points on each scattering curve. Only a fraction of data points is plotted. (b) Log-log plot of a scaled intensity curve based on the scattering curves from three different concentrations as shown in Fig. 8(a).

Same symbols as in Fig. 8(a) with  $M_w = 1.42 \times 10^5$  g/mol and  $A_2 = 3.63 \times 10^{-4}$  mL mol g<sup>-2</sup>. Again only a small fraction of data points are plotted. (Reproduction of Fig. 8 of Ref. 77)

noted that the scattering curves are slightly curved. Figure 8(b) shows a log-log plot of scaled scattered intensities of the three scattering curves of Figure 8(a). Overlapping of the three scattering curves with zero adjustable parameters is clearly demonstrated. The results for  $d_K$ , as well as the exponent  $\beta$  related to the coil behavior between the entanglement points, are listed in Table II. It should be noted that our  $d_K$  values represent the fractal dimension of swollen branched epoxy polymers in solution. The variable  $Y$  in Table II represents a correlation length  $\xi$  below which the polymer coil behavior should begin to dominate. Based on the values of constant  $d_f$ , we see a cut off value of  $Y^{-1} \approx 20 \text{ \AA}$  with  $d_K \approx 2.17$  for samples 6 to 13. At earlier polymerization stages, we consider the branched polymer chains to have lower  $d_f$  values with  $\xi$  no longer related closely to the polymer mesh size. Figure 9 shows a more quantitative approach to determine the mesh

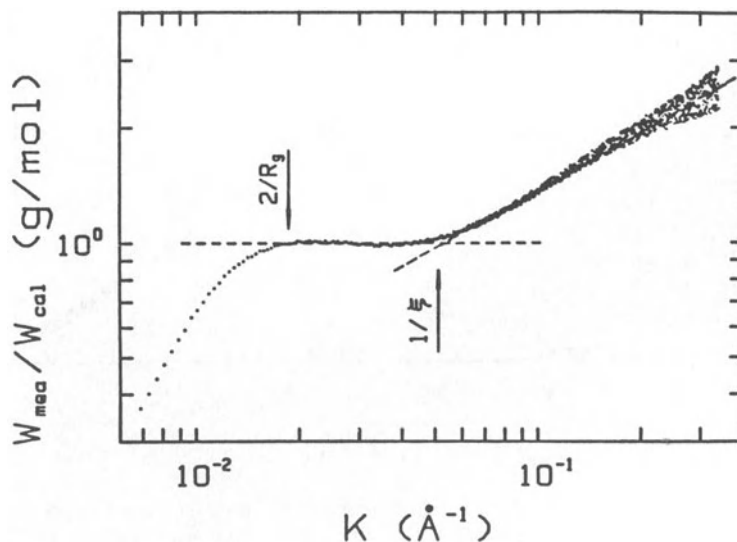


Figure 9. Plot of  $W_{\text{mea}}/W_{\text{cal}}$  versus  $K$  for sample 7.  $M_w = 5.00 \times 10^4$  g/mol,  $R_g = 105 \text{ \AA}$ .  $W_{\text{mea}} = (I/H'C)_{\text{mea}, C=0}$ .  $W_{\text{cal}} = 3.01 K^{-2.17}$ . Slope (at  $K > 1/\xi$ ) =  $0.49 \pm 0.06$ . (Reproduction of Fig. 9 of Ref. 77)

size  $\xi$  ( $\approx 19.2 \pm 3.0 \text{ \AA}$ ) and to show the deviation of the measured curve from  $W_{\text{cal}}(\text{g/mole}) = 3.01 K^{2.17}$  with  $K$  expressed in  $\text{\AA}^{-1}$  for sample 7. The results are listed in Table III. As the  $K$ -range obeying the fractal dimension  $d_K$  is limited, the range of  $K$  used in the determination of  $d_K$  should always be considered with care.

Beyond the mesh size range ( $K > \xi^{-1}$ ), we have noted an epoxy polymer coil behavior with  $I(K) \sim K^{-\beta}$  and  $\beta \approx 1.68 \pm 0.06$ , as listed in Table II(b). The value  $(d_f - \beta) = 2.17 - 1.68 = 0.49$  is the slope shown in Fig.

9 for  $K > \xi^{-1}$ . Daoud and Joanny<sup>44</sup> predicted a linear blob behavior of  $\beta \sim 5/3$  in a theta solvent.

We now come to the determination of  $d_R$ . A log-log plot of  $\langle R_g^2 \rangle_z^{1/2}$

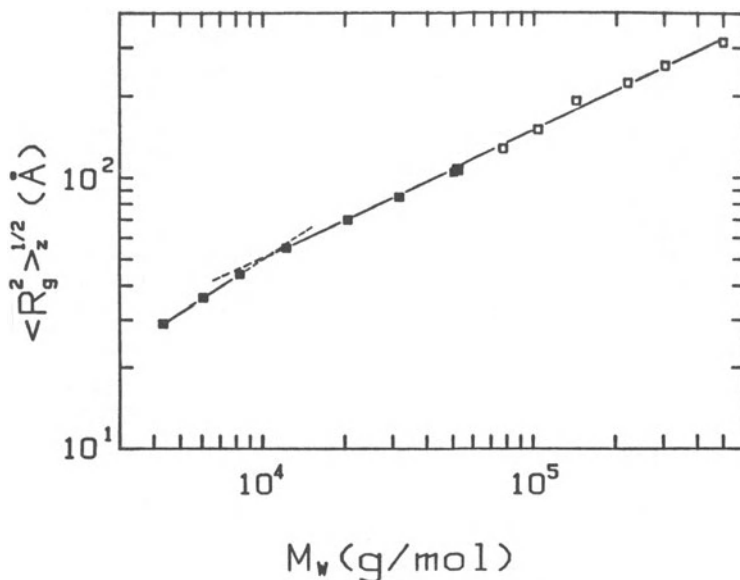


Figure 10. Log-log plot of  $\langle R_g^2 \rangle_z^{1/2}$  versus  $M_w$ . Solid squares denote SAXS measurements while hollow squares denote light scattering measurements.  $M = k_R R_g^d$  with  $R_g$  and  $M$  expressed in units of  $\text{\AA}$  and  $\text{g/mol}$ , respectively.

| Fitting range     | $k_R$                       | $d_R$           |
|-------------------|-----------------------------|-----------------|
| whole (13 points) | $4.59 \pm 0.41$             | $2.00 \pm 0.03$ |
| 3 low points      | $(2.38 \pm 0.15) \times 10$ | $1.55 \pm 0.02$ |
| 10 higher points  | $3.04 \pm 0.33$             | $2.07 \pm 0.04$ |
| 9 higher points   | $3.25 \pm 0.76$             | $2.06 \pm 0.05$ |

(Reproduction of Fig. 10 of Ref. 77)

versus  $M_w$ , as shown in Figure 10, reveals a slight curvature in the low molecular weight region, i.e., during the initial stages of the curing process, the epoxy polymer appears to have different structures from those at later stages even before the gelation threshold. The experimental results shown in Figure 10 required a combination of SAXS (denoted by solid squares) and LLS (denoted by hollow squares) measurements. Although a least-squares fitting of all the data points using  $\langle R_g^2 \rangle_z^{1/2} = k_R M_w^{\alpha_R}$  with  $d_R = 1/\alpha_R$  shows a reasonable  $d_R = 2.0$ , we have approximated the slight curvature at low  $R_g$  values by breaking the curve into two straight sections near  $M_w \sim 1 \times 10^4$  g/mol. Least squares fitting of the first three and four low  $M_w$  data points yields  $d_R \sim 1.55$  and 1.61, respectively, while  $d_R (=d_f) \sim 2.05$  for the ten higher  $M_w$  data points. Thus, the concept of self-similar fractals should not be applied uniformly to the epoxy polymer product in the very beginning of the curing process for our epoxy system.

It is interesting to note that the difference in scattering curves for low molecular weight and for high molecular weight epoxy polymers appears to occur at a fairly high molecular weight of  $\sim 10^4$  g/mole. We speculate that the reason for this behavior is due to the relatively low catalyst concentration of  $\sim 0.1\%$ , i.e., there is only one catalyst molecule for about one thousand epoxy monomers. During the initial polymerization process, most of the epoxy polymers are relatively linear because the branching probability is fairly small.

From our light scattering intensity measurements we have also

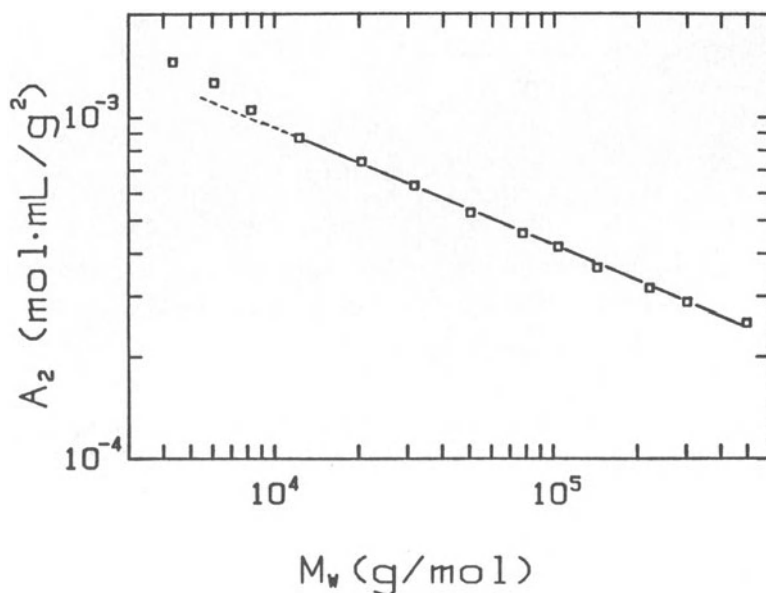


Figure 11. Log-log plots of  $A_2$  versus  $M_w$  from light scattering intensity measurements.  $A_2 = k_A M_w^{\alpha_A}$  with  $A_2$  and  $M$  in units of mol mL/g<sup>2</sup> and g/mol, respectively.

| Fitting range     | $k_A$                            | $\alpha_A$       |
|-------------------|----------------------------------|------------------|
| whole (13 points) | $(3.02 \pm 0.31) \times 10^{-2}$ | $-0.37 \pm 0.01$ |
| 10 higher points  | $(2.19 \pm 0.13) \times 10^{-2}$ | $-0.34 \pm 0.01$ |

(Reproduction of Fig. 11 of Ref. 77)

determined the second virial coefficient  $A_2$  according to Eq. (1). Figure 11 shows a log-log plot of  $A_2$  versus  $M_w$ . We have noted a curvature at low values of  $M_w$ , similar to the trend exhibited in Figure 10. By using

$$A_2 = k_A M_w^{\alpha_A} \quad (7)$$

we get  $k_A = (3.02 \pm 0.31) \times 10^{-2}$  and  $(2.19 \pm 0.13) \times 10^{-2}$  as well as  $\alpha_A = -0.37 \pm 0.01$  and  $-0.34 \pm 0.01$ , respectively, with all 13 data points and the 10 higher molecular weight data points. We are not aware of experimental determinations for the constants  $k_A$  and  $\alpha_A$  in highly branched polymers. However, experimental results on star-branch polymers suggest an  $\alpha_A$  value of  $-0.37$  for 12-arm and 18-arm polystyrene stars,<sup>45</sup> in fairly good agreement with our findings.

The results of  $A_2$  suggest that the lower  $M_w$  epoxy polymers are more swollen than the higher  $M_w$  epoxy polymers during the later stages of the curing process before the gel point. This observation agrees with our concept that during the initial polymerization stages, the epoxy polymer molecules are less branched. The smaller degree of branching in the lower  $M_w$  epoxy polymers permits easier swelling of the polymer molecules. With increasing molecular weight, the polymer molecules become more highly branched and less swollen. The concept of fractal geometry is applicable because of the agreement between  $d_R (-d_f) - 2.05$  over a substantial range of reaction time before the gel point, as shown in Table II and Fig. 10.

Beyond the gelation threshold, SAXS can be used to determine the fractal geometry of epoxy polymers as shown typically in Fig. 12. For the present epoxy system, we still require immersion of the gel particles in MEK in order to increase the electron density difference.

$d_f \sim 2.14 \pm 0.02$  and  $2.13 \pm 0.03$  for  $K \leq 1/30 \text{ \AA}^{-1}$  and  $K \leq 1/20 \text{ \AA}^{-1}$ , respectively.

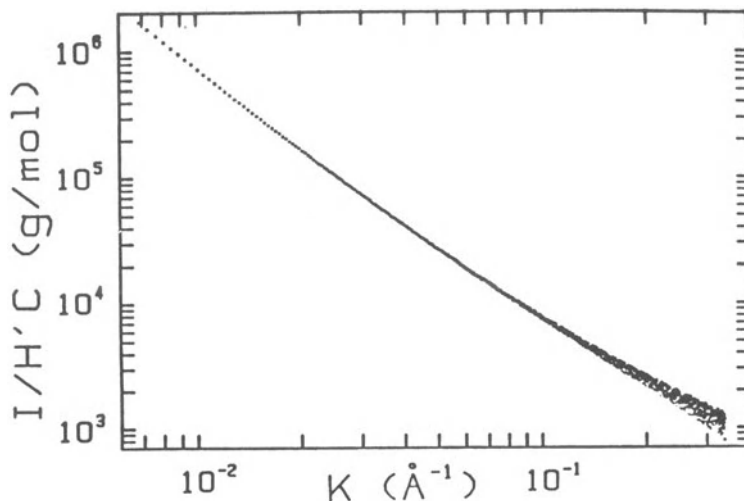


Figure 12. Log-log plots of  $I/H'C$  versus  $K$ . The epoxy gel was swollen in MEK. Least squares fitting of 817 data points to  $I \propto K^\alpha$  yields  $\alpha = 2.14 \pm 0.02$  and  $1.69 \pm 0.05$  for  $K \leq 1/30 \text{ \AA}^{-1}$  and  $1/30 \leq K \leq 1/4 \text{ \AA}^{-1}$ , respectively. (Reproduction of Fig. 13 of Ref. 77)

The linear behavior as shown in Fig. 8(b), the horizontal region as shown clearly in Fig. 9, and our knowledge on the molecular weight distribution as shown in Fig. 12, strengthen the supposition of Eq. (5), i.e., we have a  $K$ -region with a constant  $d_K$  in the polydisperse epoxy polymer and  $d_R$  can be evaluated over a broad enough  $M_w$  range even if the epoxy polymers are polydisperse.

### 3.5. Molecular Weight Distribution of Branched Epoxy Polymer

3.5.1. Laplace Transform. By following the experimental procedures for self-beating and baseline considerations, we could obtain precise measurements of the intensity-intensity time correlation function  $G^{(2)}(K, \tau)$ :

$$G^{(2)}(K, \tau) = A (1 + b |g^{(1)}(K, \tau)|^2) \quad (8)$$

where the baseline  $A$  agreed with the measured baseline  $\lim_{\tau \rightarrow \infty} G^{(2)}(K, \tau)$  to

within about 0.1%. Figure 13 shows a typical experimental intensity-intensity photoelectron count autocorrelation function for the epoxy

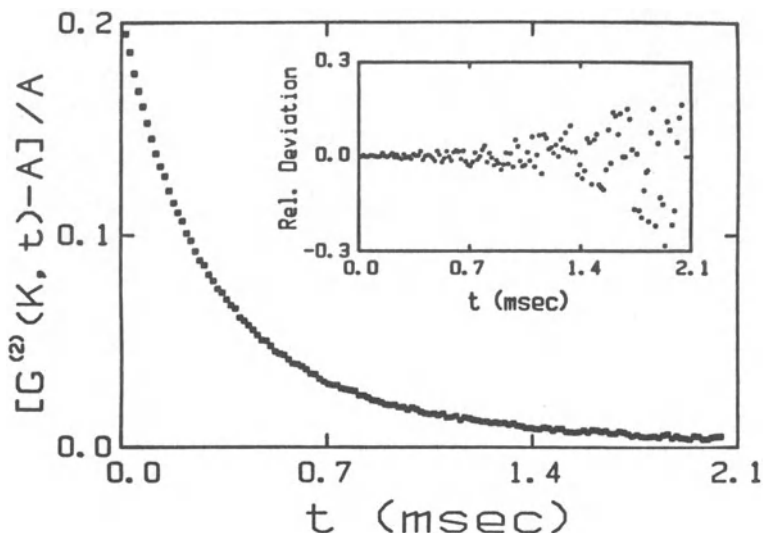


Figure 13. A typical unnormalized Intensity-intensity photo-electron count autocorrelation function.  $1.11 \times 10^{-4}$  g/mL of epoxy polymer sample 13 ( $M_w = 4.97 \times 10^5$ ) in MEK measured at  $\theta = 30^\circ$

and  $25^\circ\text{C}$  using a delay time increment  $\Delta\tau = 15 \mu\text{sec}$ . The insert is relative deviation of the measured and the computed time correlation function using the MSVD method. Relative deviation is defined as

$$1 - \frac{[b|g^{(1)}(t)|^2]_{\text{calc.}}}{[b|g^{(1)}(t)|^2]_{\text{meas.}}}$$

(Reproduction of Fig. 1 of Ref. 61)

polymer in MEK measured at  $\theta = 30^\circ$  and  $25^\circ\text{C}$  using a delay time increment  $\Delta\tau$  of  $15 \mu\text{sec}$  and relative deviation of the measured and the computed time correlation function by using the MSVD method of Laplace inversion.

The MSVD technique<sup>46,47,48</sup> has been described in detail elsewhere. We outline only the essential steps which are necessary in describing our data fitting results. In the MSVD technique, we do Laplace inversion of the electric field time correlation function:

$$g^{(1)}(K, \tau) = \int_0^\infty G(K, \Gamma) e^{-\Gamma(K)\tau} d\Gamma \quad (9)$$

by approximating  $G(\Gamma)$  with a set of linearly or logarithmically spaced single exponentials:

$$G(\Gamma) = \sum_j P_j \delta(\Gamma - \Gamma_j) \quad (10)$$

where  $g^{(1)}(\tau_i) = b_i = \sum_j P_j \exp(-\Gamma_j \tau_i)$  with  $P_j$  being the weighting factors of the  $\delta$  function measured at scattering vector  $K$ . The validity of the MSVD method has been tested previously.<sup>47-50</sup>

We have to stress here that, in an ill-posed problem, goodness of fitting does not guarantee a correct solution to the inversion. However, the validity of the MSVD method for a unimodal characteristic line-width distribution has been tested thoroughly by using simulated data and known polymer systems under comparable experimental conditions, counting rates and statistics. Figure 14 shows typical line-width distributions

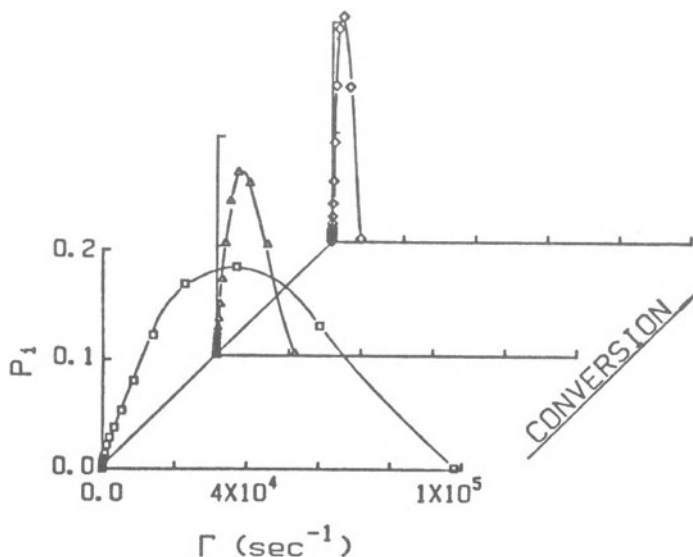


Figure 14. Plots of  $P_j$  versus  $\Gamma$  for epoxy polymer sample 1, sample 9 and

sample 13 in MEK at  $\theta = 30^\circ$  and  $25^\circ\text{C}$  based on the MSVD method.

| Sample | Notation         | $M_w$ (g/mol)      | $\bar{\Gamma}$ (sec <sup>-1</sup> ) | $\mu_2/\bar{\Gamma}^2$ |
|--------|------------------|--------------------|-------------------------------------|------------------------|
| 1      | Hollow squares   | $4.32 \times 10^3$ | $2.29 \times 10^4$                  | 0.63                   |
| 9      | Hollow triangles | $1.03 \times 10^5$ | $3.98 \times 10^3$                  | 0.45                   |
| 13     | Hollow diamonds  | $4.97 \times 10^5$ | $1.79 \times 10^3$                  | 0.40                   |

(Reproduction of Fig. 2 of Ref. 61)

obtained by the MSVD method. In Figure 14, we clearly see that the characteristic line-width shifts to lower frequencies and the distributions become narrower with increasing % of conversion. Numerical results of the transform by the MSVD method for a set of epoxy polymers at different % conversions are listed in Table IV. It should be noted that discrete ( $P_j$ s) and continuous ( $G(\Gamma)$ ) normalized characteristic

line-width distributions are not the same. In a discrete distribution in terms of  $P_j$ 's, we have Eq. (10). If  $\Gamma_j$  does not have equal spacing, which is indeed the case for our MSVD method,  $P_j$  has to be rescaled in order to convert it to a continuous distribution  $G(\Gamma)$ , i.e.  $G(\Gamma) \neq G(\ln\Gamma)$ . The rescaling is approximately done by using  $G(\Gamma_j) = P_j / \Gamma_j$ .

In order to transform the measured characteristic line-width distribution at finite angle and finite concentration to a molecular weight distribution, we have to know how the characteristic line-width  $\Gamma$  depends on the scattering angle (or  $K$ ) and the polymer concentration. We experimentally determined such a relation by using

$$\bar{\Gamma} = \bar{D}_0^0 K^2 (1 + f R_g^2 K^2) (1 + k_d C) \quad (11)$$

where  $f$  is a dimensionless number and depends on chain structure, polydispersity and solvent quality, and  $k_d$  is the second virial coefficient for diffusion. Figure 15 shows a typical  $K^2$  dependence of

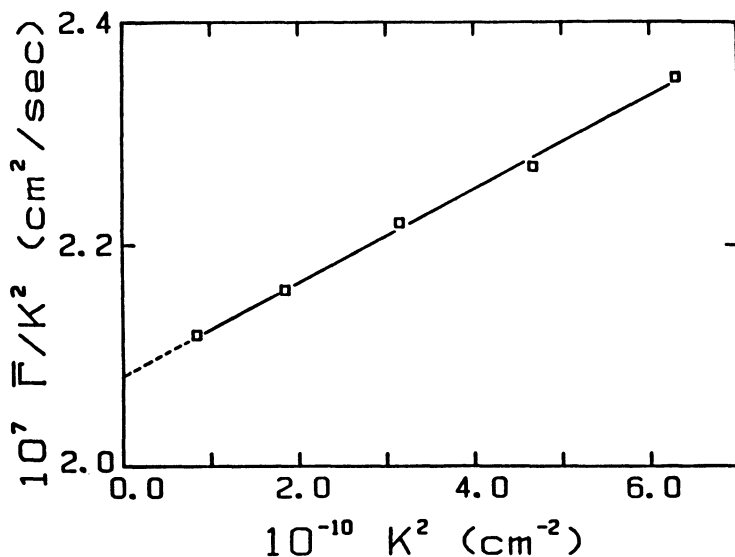


Figure 15. Plots of  $\bar{\Gamma}/K^2$  versus  $K^2$  for epoxy polymer 13 ( $M_w = 4.97 \times 10^5$  and  $\langle R_g^2 \rangle_z^{1/2} = 31.4 \text{ nm}$ ) in MEK at  $25^\circ\text{C}$  and  $\lambda_o = 488 \text{ nm}$ . The straight line represents

$$\bar{\Gamma}/K^2 = 2.08 \times 10^{-7} (1 + 0.19 \langle R_g^2 \rangle_z K^2)$$

(Reproduction of Fig. 3 of Ref. 61)

the z-average characteristic line-width  $\bar{\Gamma}$ . Figure 16 shows a typical

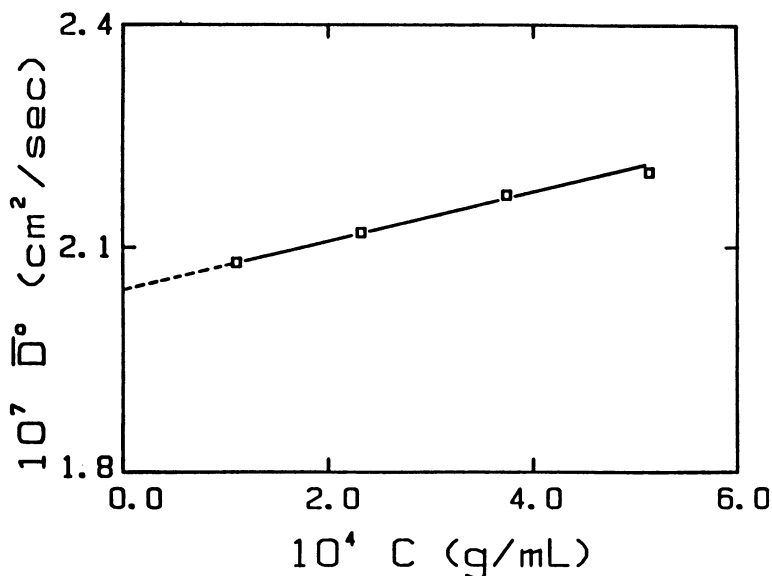


Figure 16. Plots of  $\bar{D}^0$  ( $= \lim_{K \rightarrow 0} \bar{\Gamma}/K^2$ ) versus concentrations ( $C$ ) for the same sample in Figure 15. The straight line represents  $\bar{D}^0 = 2.05 \times 10^{-7} (1 + 1.41 \times 10^2 C)$  (Reproduction of Fig. 4 of Ref. 61)

concentration dependence of the translational diffusion coefficient  $\bar{D}^0$  ( $= \lim_{K \rightarrow 0} \bar{\Gamma}/K^2$ ). The  $k_d$  and  $f$  values are also listed in Table IV. After having obtained  $k_d$  and  $f$ , we can convert  $G(\Gamma)$  versus  $\Gamma$  to  $G(D_o^0)$  versus  $D_o^0$ . Further, we can calculate the z-average translational diffusion coefficient  $\bar{D}_o^0$  at each reaction stage, as listed in Table IV. By using the  $\bar{D}_o^0$  and the Stokes-Einstein relation:  $D = \frac{k_B T}{6\pi\eta R_h}$ , we can calculate the equivalent hydrodynamic radius  $R_h$ .

3.5.2. Conversion from  $G(\Gamma)$  to  $F_w(M)$ . In previous publications,<sup>48-50</sup> we converted the line-width distribution  $G(\Gamma)$  to the weight average molecular weight distribution  $F_w(M)$  by using an experimentally

determined scaling relation  $\bar{D}_o^\circ = k_D M_w^{-\alpha_D}$  where  $\bar{D}_o^\circ$  and  $M_w$  are the z-average translational diffusion coefficient extrapolated to infinite dilution and the weight average molecular weight, respectively. A log-log plot of  $\bar{D}_o^\circ$  versus  $M_w$  is shown on Figure 17. We find that the data

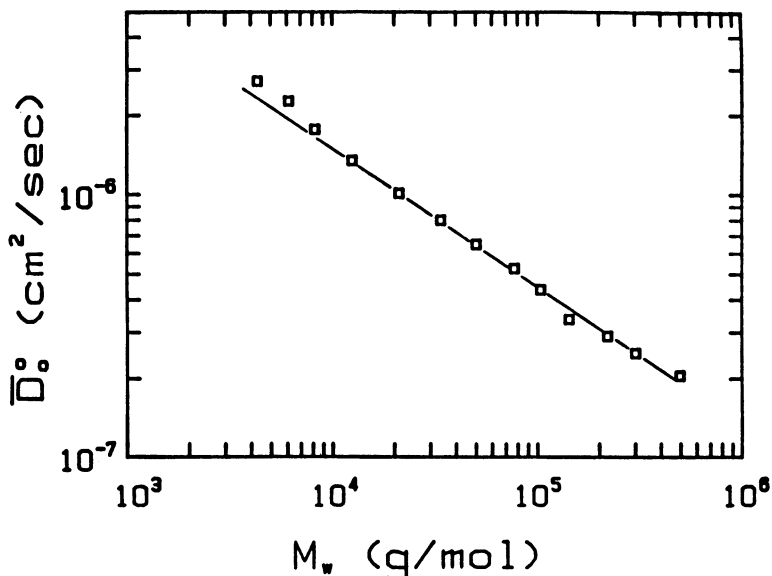


Figure 17. log-log plot of translational diffusion coefficient  $\bar{D}_o^\circ$  versus  $M_w$  for the epoxy polymer in MEK at 25° and  $\lambda_o = 488$  nm. The straight line represents  $\bar{D}_o^\circ = 1.56 \times 10^{-4} M_w^{-0.508}$  with  $\bar{D}_o^\circ$  and  $M_w$  in units of cm<sup>2</sup>/sec and g/mol, respectively. (Reproduction of Fig. 7 of Ref. 61)

can be represented by a straight line if we disregard the first three data points during the initial stages of the curing process. From Fig. 17, we calculated  $k_D = (1.56 \pm 0.20) \times 10^{-4}$  and  $\alpha_D = 0.508 \pm 0.011$  with  $\bar{D}_o^\circ$  and  $M_w$  expressed in units of cm<sup>2</sup>/sec and g/mol, respectively. In fact, the  $\Gamma$  to  $M$  conversion should use the scaling relation  $D_o^\circ = k_D M^{-\alpha_D}$  and the condition  $\Gamma = DK^2$  based on monodisperse fractions. The  $k_D$  and  $\alpha_D$

obtained from  $\bar{D}_o^o$  and  $M_w$  are approximations to the true values since we usually do not have monodisperse polymer samples to establish the scaling relation. In other words, the narrower the molecular weight distributions of calibration samples over the same molecular weight range, the better the approximation becomes. So, the standard calibration method requires a set of narrow molecular weight distribution polymers of different molecular weights. It is very difficult to apply this calibration procedure to study the branched epoxy polymers because all epoxy polymers are very polydisperse. Thus, we need to examine the calibration problem from a slightly different viewpoint in order to achieve the conversion as precisely as possible. We applied the following procedure for a more precise determination of  $k_D$  and  $\alpha_D$ .

For polydisperse polymer,

$$\int_0^\infty G(D_o^o) dD_o^o = \int_0^\infty F_z(M) dM = 1 \quad (12)$$

where  $F_z(M)$  is the z-weighted molecular weight distribution function. By accepting the scaling relation  $D_o^o = k_D M^{-\alpha_D}$ , we finally obtain

$$M_w = \frac{k_D^{1/\alpha_D} \int G(D_o^o) dD_o^o}{\int G(D_o^o) D_o^o^{1/\alpha_D} dD_o^o} \quad (13)$$

With two polymer samples of different molecular weight and distribution but obeying the same  $k_D$  and  $\alpha_D$ , we have two  $G(D_o^o)$ , denoted by  $G_1(D_o^o)$  and  $G_2(D_o^o)$ . From them, we could calculate two  $(M_w)_{\text{calc}}$ , denoted by  $(M_{w,1})_{\text{calc}}$  and  $(M_{w,2})_{\text{calc}}$ . The ratio of  $(M_{w,1})_{\text{calc}}$  and  $(M_{w,2})_{\text{calc}}$  is

$$\frac{(M_{w,1})_{\text{calc}}}{(M_{w,2})_{\text{calc}}} = \frac{[\int G_1(D_o^o) dD_o^o] [\int G_2(D_o^o) D_o^o^{1/\alpha_D} dD_o^o]}{[\int G_2(D_o^o) dD_o^o] [\int G_1(D_o^o) D_o^o^{1/\alpha_D} dD_o^o]} \quad (14)$$

where  $k_D$  has been cancelled out. The two calculated  $(M_w)_{\text{calc}}$  values have to equal the two measured  $M_w$  values. It means that we already know the value of left side of Eq. (14) experimentally. Now, we vary the value of  $\alpha_D$  and calculate the right side of Eq. (14) until the left side equals

to the right side. In this way, we are able to find the correct  $\alpha_D$  value from two polymer samples with different and broad MWD. After we have determined  $\alpha_D$ , we can determine the  $k_D$  value by using Eq. (13). The above procedure can be expanded easily to  $N$  samples of different molecular weight and distribution. After having determined the correct values of  $k_D$  and  $\alpha_D$ , we can use the scaling relation  $D_o^o = k_D M^{-\alpha_D}$  (not  $\bar{D}_o^o = k_D M_w^{-\alpha_D}$ ) to convert  $G(D_o^o)$  versus  $D_o^o$  to  $F_w(M)$  versus  $M$ .

By using the method presented above, we obtained that  $k_D = (2.14 \pm 0.32) \times 10^{-4}$  and  $\alpha_D = 0.527 \pm 0.013$ . The  $k_D$  and  $\alpha_D$  obtained from average values of  $M_w$  and  $\bar{D}_o^o$ , as shown in Fig. 17, are different from the results obtained from  $M$  and  $D_o^o$ , which is not surprising because our epoxy polymers are quite polydisperse.

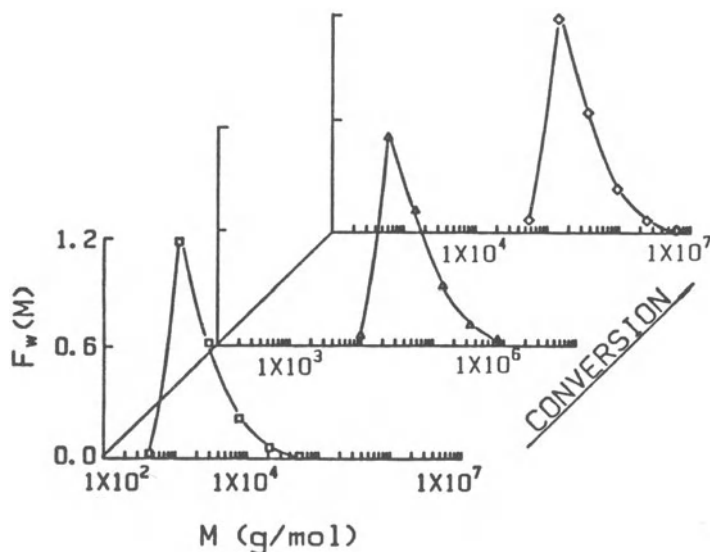


Figure 18. Typical plots of weight distributions for the same samples in Figure 14.

| Sample | Notation         | $M_w$ (g/mol)      | $M_n$ (g/mol)      | $M_w : M_n$ |
|--------|------------------|--------------------|--------------------|-------------|
| 1      | Hollow squares   | $4.32 \times 10^3$ | $1.30 \times 10^3$ | 3.32        |
| 9      | Hollow triangles | $1.03 \times 10^5$ | $3.99 \times 10^4$ | 2.58        |
| 13     | Hollow diamonds  | $4.97 \times 10^5$ | $2.00 \times 10^5$ | 2.49        |

(Reproduction of Fig. 8 of Ref. 61)

Having computed  $G(D_o^0)$  versus  $D_o^0$ , we now make use of the relation  $D_{o,j}^0$  (in  $\text{cm}^2/\text{sec}$ ) =  $2.14 \times 10^{-4} M_j^{-0.527}$  for each fraction of the epoxy polymer having molecular weight  $M_j$  (in g/mole). At each scattering angle, the excess Rayleigh ratio has the form:  $R_{VV}(K) \propto \sum_j F_w(M_j) M_j P(M_j, K) \propto \sum_j P_j$ , where  $P(M, K)$  is the particle scattering factor and  $F_w(M)$  is the normalized weight distribution for the epoxy polymers. The  $\propto$  sign denotes that we are not concerned with the proportionality constant. At small enough scattering angles,  $P_j \propto F_w(M_j) M_j P(M_j, K) \approx F_w(M_j) M_j$  as  $P(M_j, K) \approx 1$ . The first-order term for  $P(M_j, K)$  has the form  $P(M_j, K) \approx 1 - \langle R_g^2 \rangle_{z, M_j} K^2 / 3$ . Thus, we can correct for the interference

effect in the molecular weight distribution whenever it is necessary since we have the empirical scaling relation between the radius of gyration and the molecular weight, as shown in 3.4.

Figure 18 shows three typical normalized weight distributions of the epoxy polymers at three different % conversions. In Fig. 18, we have ignored the very high molecular weight tails on the distribution curves because of noise and background uncertainties. The contribution of the high molecular weight tail to the cumulative molecular weight distribution is less than 1% of the total weight fraction. From the  $F_w$  distributions, we can calculate  $M_w : M_n$ , which represents the polydispersity of each epoxy polymer sample. The results of  $M_w : M_n$  for 13 samples at different % conversion are shown on Figure 19. It is noted

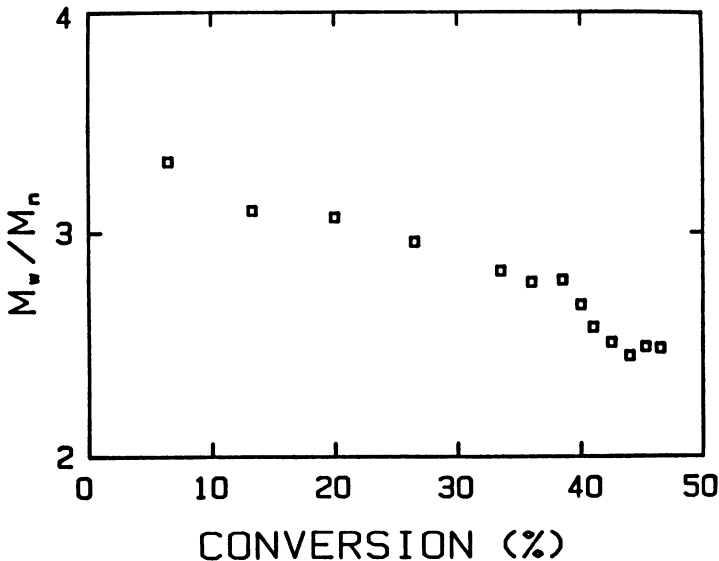


Figure 19. Plot of  $M_w:M_n$  versus extent of conversion for 13 epoxy polymers at different reaction stages.  $M_w:M_n$  were determined by using the MSVD method. (Reproduction of Fig. 10 of Ref. 61)

that the values of  $M_w:M_n$  become smaller with increasing reaction time, suggesting that the polydispersity of the branched epoxy polymer product during the initial stages is much higher than that at the later stages near the gelation threshold. We also observed that  $M_w:M_n$  approaches a constant value of  $\approx 2.5$  as the polymerization approaches the gelation threshold.

3.5.3. SEC measurements and Comparison with LLS. In order to check our determination of the molecular weight distribution by means of LLS, we used the same samples for SEC experiments. There are many calibration methods for the SEC column.<sup>51-60</sup> However, for branched polymers and rod-like polymers, conventional calibration methods do not apply. All reported calibration methods require at least two polymers with different molecular weights, or one sample with either two different molecular weight averages or one molecular weight plus intrinsic viscosity data, implying the use of one more instrument, such as an osmometer or a viscometer. In laser light scattering, we need only one broad MWD polymer sample and one instrument (i.e. LLS) to calibrate the SEC column. The details have been described elsewhere.<sup>61</sup> Figure 20 shows

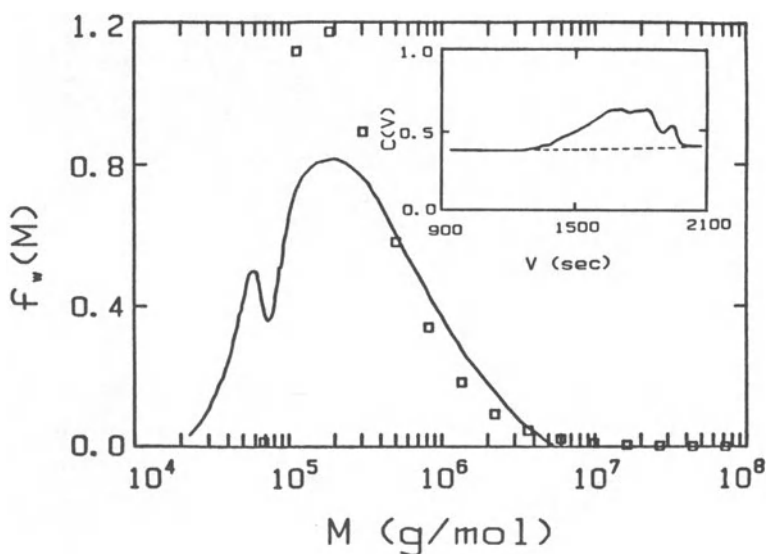


Figure 20. Comparison of the weight distributions  $F_w(M)$  obtained for the same epoxy polymer ( $M_w = 4.97 \times 10^5$  g/mole) by using the SEC experiment (continuous line) and the LLS experiment (hollow squares). (Reproduction of Fig. 11 of Ref. 61)

plots of  $F_w(M)$  versus  $M$  with  $F_w(M)$  from SEC denoted by the continuous line and those from LLS denoted by hollow squares. The agreement is reasonable especially if we take into account of the facts that LLS emphasizes on larger particles and SEC emphasizes on particle weight fractions.  $F_w(M)$  from SEC showed a small peak around molecular weight  $6 \times 10^3$ , which was not observed in  $F_w(M)$  from LLS. This discrepancy is not surprising because signals from LLS not only emphasized large particles but our MSVD Laplace inversion technique is designed for unimodal characteristic line-width distribution analysis. We also tried to use the CONTIN algorithm. However, with an estimated intensity ratio of only a few percent for the small to large peak ratio from SEC and a molecular weight separation of about a factor of 4 for the two peaks, it is reasonable to find that LLS failed to resolve the two peaks. The low molecular weight peak as revealed by SEC tells us additional kinetics information about the formation of the epoxy polymer network, which will be discussed in a separate article. By comparing the two MWDs from LLS and SEC, we note that  $M_w : M_n$  ( $\approx 3.0$ ) by SEC is larger than the value ( $\approx 2.5$ ) obtained from LLS.

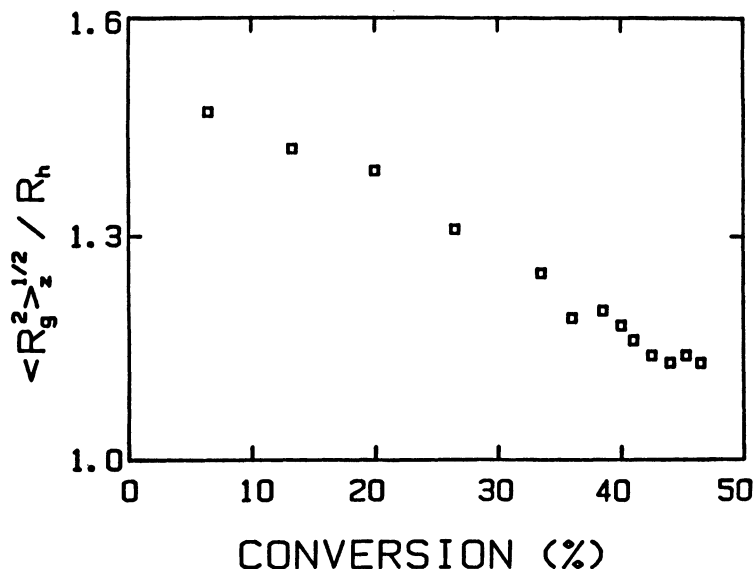


Figure 21. Plot of  $\langle R_g^2 \rangle_z^{1/2} / R_h$  for 13 epoxy polymer samples at different reaction stages. (Reproduction of Fig. 12 of Ref. 61)

Figure 21 shows the ratios of the z-average root-mean-square radius of gyration and the hydrodynamic radius,<sup>62</sup>  $\rho = R_g/R_h$ , for the 13 epoxy polymer samples which we extracted during different reaction stages.  $\rho$  does not depend on the bond length and the degree of copolymerization but is a function of the branching density and polydispersity. For a linear polymer coil,  $R_g/R_h \approx 1.504$ . For a highly branched polymer with monodisperse primary coil chain distribution, the value of  $R_g/R_h$  decreases to 1.130.<sup>63,64</sup> In Table 1 of reference 63, the calculated values of  $\rho$  changed from 1.5044 to 1.1657 for polymers with the degree of branching changed from 1 (linear polymer) to 100, respectively. The value of  $R_g/R_h$  ratio obtained from our experimental results changed from 1.47 to 1.14 as the reaction approaches the gel point. The change in  $R_g/R_h$  ratio tells us that the epoxy polymer behaves close to a linear random coil during the initial reaction stages. The degree of branching increases as the polymerization reaction approaches the gel point.

The evolution of the molecular weight distribution function during the gelation transition is related to the spectacular variation of macroscopic properties of a crosslinked polymer system.<sup>65,66</sup> There are only small molecules inside the reaction bath at the initial reaction stage. Near the gelation threshold, a macroscopic cluster as well as precursor units and clusters of all intermediate sizes are formed. Various statistical and kinetic models have been proposed to describe the evolution of the molecule weight distribution for different gelation processes.<sup>65-70</sup> They all show that the molecular weight distribution of large clusters near the gelation threshold can be written in a scaling form.<sup>71</sup>

$$N(M, \epsilon) \approx M^{-\tau} f(M/M^*(\epsilon)) \quad (15)$$

where,  $N(M, \epsilon)$  is the number of clusters with molecular weight  $M$  when the relative distance from the gel point is  $\epsilon$ .  $\epsilon = |p - p_c|$ , where  $p$  is the extent of conversion and  $p_c$  is the extent of conversion at the gelation threshold. Eq. (15) implies that the number of clusters decreases as a power law of molecular weight with a critical exponent  $\tau$ . Before the gelation threshold, a typical molecular weight  $M^*(\epsilon)$  exists in the molecular weight distribution, which limits the spread of the distribution and which diverges when the gel threshold is approached:  $M^* \approx \epsilon^{-1/\sigma}$  where  $1/\sigma$  is a constant which is sometimes referred to as the

gap exponent. The crossover function  $f(x)$  describes the cutoff of the distribution for large molecules greater than  $M^*$ . Leibler, L. and Schosseler, F. experimentally demonstrated<sup>72</sup> a direct quantitative method of measuring the typical molecular weight ( $M^*$ ) from light-scattering spectra. They showed that the molecular weight  $M_{\max}$  of molecules in the distribution given the maximum scattered light intensity provides a measure of the cutoff molecular weight and can be identified with the typical molecular weight  $M^*$ . They also experimentally showed that if Eq. (15) holds for the molecular weight distribution of branched polymer molecules, the function

$$G(M/M_{\max}) = M_{\max}^{\tau-1} \phi(M, t) \approx (M/M_{\max})^{1-\tau} f(M/M_{\max}) \quad (16)$$

is a universal function of  $M/M_{\max}$  independent of the advancement of the reaction,  $t$ . Eq. (16) is valid for the high molecular weight  $M$  for which  $\phi(M, t)$  is expected to be independent of the initial molecular weight distribution.  $\tau$  in Eq. (16) cannot take an arbitrary value since Eq. (16) implies that the weight-average molecular weight  $M_w$  varies like

$$M_{\max}^{3-\tau}$$

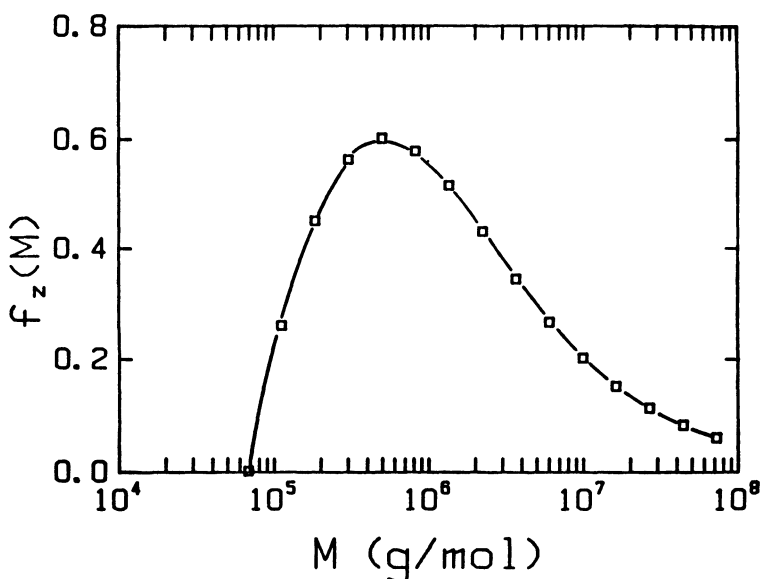


Figure 22. Plot of  $f_z(M)$  versus  $M$ , based on  $F_w(M)$  versus  $M$  data from LLS in Fig. 21.  $M_{\max}$  is determined from the location of  $M$  at which  $(f_z(M))_{\max}$  occurs. (Reproduction of Fig. 13. of Ref. 61)

The scattered intensity ( $I$ ) can be written as

$$I = \int_0^{\infty} I(M) dM \propto \int_0^{\infty} f_n(M) M^2 dM = \int_0^{\infty} f_z(M) dM \quad (17)$$

where  $I(M)$  is the scattered intensity from the fraction of polymer with molecular weight  $M$ . Eq. (17) tells us that  $(I(M))_{\max}$  corresponds to  $(f_z(M))_{\max}$  as shown in Fig. 22. Then, the molecular weight  $M$  corresponding to  $(f_z(M))_{\max}$  should be  $M_{\max}$ . Experimentally, we measured  $M_w$  and calculated  $f_z(M)$  from the line-width measurements for different reaction stages. We obtained  $M_{\max}$  from  $(f_z(M))_{\max}$  in the distribution. A log-log plot of  $M_{\max}$  versus  $M_w$  is shown in Figure 23. The data points

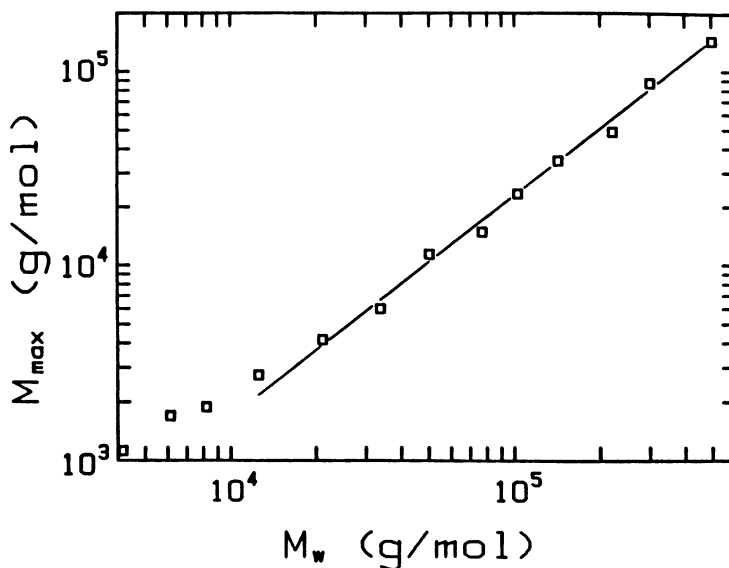


Figure 23. Log-log plot of  $M_{\max}$  versus  $M_w$ . Slope =  $(3 - \tau)^{-1} = 1.1 \pm 0.1$  and  $\tau = 2.1 \pm 0.1$ . (Reproduction of Fig. 14 of Ref. 61)

except the first three lower molecular weight values are essentially on a straight line, whose slope is  $1.1 \pm 0.1$ . From the slope, we calculated  $\tau = 2.1 \pm 0.1$ . The result further confirms the existence of a scaling law for the molecular weight distribution function in the sol phase, the main result of all theories concerned with gelation processes. Our value of the scaling constant  $\tau$  is smaller than the classical mean-field prediction  $\tau = 2.5$ , but is closer to the value of 2.3 in reference 72.

### 3.6. Branching Kinetics of Epoxy Polymerization

After having obtained the molecular weight distributions at each reaction stages, we focused our attention on the branching kinetics of the epoxy polymerization because the branching kinetics could provide a theoretical background for understanding the change of the molecular weight and its distribution with the reaction time.

The copolymerization of 1,4-butanediol diglycidyl ether (DGEb) and cis-1,2-cyclohexanedicarboxylic anhydride (CH) in the presence of benzyl dimethyl amine (CA) is dominated by alternative linkages between DGEb and CH, i.e. the reactions between the epoxy resins and between the anhydrides are suppressed.<sup>73</sup> Highly branched epoxy copolymers are formed in the copolymerization reaction because the sum of the reaction functionalities of DGEb (two epoxy rings which can form four chemical bonds) and of CH (one anhydride ring which can form two chemical bond) is six, which is larger than the gelation criterion, i.e. a minimum total of five functionalities is needed to form a branching point. Figure 5 shows graphically how the branch points are formed in the copolymerization reaction. At the initial reaction stage, most of the polymers formed are linear. As the reaction proceeds, the degree of branching of the branched epoxy copolymer increases. Finally, a three-dimensional network is formed at the gelation threshold. We know that the triamine plays a very important role in initiating the reaction because without triamine as a catalyst, the overall reaction is very slow. But, it is not clear how the triamine starts the reaction, i.e. we do not know whether the triamine molecule first reacts with the anhydride molecule or with the epoxy resin. However, if we examine only the branching process after the very initial reaction stage, it is not important for us to know the exact initial reaction mechanism. For convenience in discussion, let us adopt Fischer's initial mechanism,<sup>73</sup> i.e. the triamine molecule reacts first with the anhydride molecule to form an anion (active site) on the anhydride molecule and the anion further reacts with the epoxy ring on the epoxy resin to form another anion on the epoxy resin, and so on. So the total number of active sites (i.e. the total number of CA molecules) should be constant if we assume that the triamine molecules will not transfer and the active sites will not be terminated.

By assuming that: (1) all catalyst molecules start the polymerization reaction at the same time and have the same reactivity, and they will not be terminated or transferred; (2) the reactivity is independent of polymer chain length; (3) the number of molecules undergoing the chemical reaction is counted ignoring the size of the polymer molecules; and (4) rings do not form, then we are able to present a simplified model for the branching kinetics in the copolymerization process as follows.

Let us denote as  $EPM_n$  the epoxy polymer molecule which has  $(n - 1)$  branching points and  $n$  active sites, e.g.,  $EPM_1$  means a linear polymer molecule, as shown schematically in Figure 5. We further use  $N_n(t)$  to denote the number of  $EPM_n$  molecules at time  $t$  (e.g.,  $N_1(t)$  is the number

of linear polymer molecules at time  $t$ ) and,  $\bar{f}(\text{EPM}_n)$  to denote the average frequency with which each active site may react with  $\text{EPM}_n$  molecules at reaction time  $t$ . The average frequency  $\bar{f}(\text{EPM}_n)$  can be considered to have two multiplicative parts, consisting of (1) the total number of reacted CH molecules per active site per unit time, which should be equivalent to the rate of change of CH molecules (or the rate of change of epoxy rings) divided by the total number of active sites (i.e. the initial number of CA molecules) and (2) the probability of an active site reacting with  $\text{EPM}_n$  molecules, which should be the number of  $\text{EPM}_n$  molecules divided by the total number of molecules with epoxy rings (i.e. the sum of the unreacted epoxy resin molecules and the epoxy polymer molecules). If two CH molecules react with the same single DGEb molecule instead of two DGEb molecules, it will form one branching point and consume one less DGEb molecule. So the number of unreacted epoxy resin molecules should be the difference between the initial number of the epoxy resin molecules and the number of reacted epoxy rings plus the total number of branching points. In this way,  $\bar{f}(\text{EPM}_n)$  can be expressed as

$$\bar{f}(\text{EPM}_n) = \frac{-dN_{\text{CH}}/dt}{N_{\text{CA}}(0)} \frac{N_n}{N_{\text{DGEb}}(0) - pN_{\text{CH}}(0) + N_b + N_{\text{EPM}}} \quad (18)$$

where  $N_{\text{CH}}(0)$ ,  $N_{\text{CA}}(0)$  and  $N_{\text{DGEb}}(0)$  are, respectively, the number of CH, CA and DGEb molecules at time  $t = 0$ .  $N_{\text{CH}}$  is the number of unreacted CH molecules at time  $t$ . The  $p$  [ $= 1 - N_{\text{CH}}/N_{\text{CH}}(0)$ ] is the CH extent of conversion. The minus sign "-" corresponds to the rate of change of CH molecules being positive because  $dN_{\text{CH}}/dt$  is always negative.  $N_{\text{EPM}}$  is the total number of epoxy polymer molecules.  $N_b$  is the total number of branching points on all the epoxy polymers.

$$N_b = \sum_{i=1}^{\infty} (i-1)N_i = \sum_{i=1}^{\infty} iN_i - \sum_{i=1}^{\infty} N_i = N_{\text{CA}}(0) - N_{\text{EPM}} \quad (19)$$

By replacing  $N_b$  in Eq. (18) with Eq. (19) and  $p$  with the definition, we get

$$\bar{f}(\text{EPM}_n) = \frac{-dN_{\text{CH}}/dt N_n}{N_{\text{CA}}(0)N_{\text{CH}}(0)[\beta - 1 + N_{\text{CH}}/N_{\text{CH}}(0)]} \quad (20)$$

where  $\beta = [N_{\text{DGE B}}(0) + N_{\text{CA}}(0)] / N_{\text{CH}}(0)$ . At a fixed initial molar ratio of epoxy resin to anhydride and temperature (T),  $\bar{f}(\text{EPM}_n)$  is a function of catalyst concentration and reaction time t or the extent of conversion p. Now let us consider the reaction frequency of a pair of epoxy polymer molecules ( $\text{EPM}_i$  and  $\text{EPM}_j$ ). As we mentioned before, an  $\text{EPM}_n$  molecule has n active sites. So the frequency for  $N_i$   $\text{EPM}_i$  molecules reacting with the  $N_j$   $\text{EPM}_j$  molecules should be  $iN_i\bar{f}(\text{EPM}_j)$  under the assumptions we have made here. In the same way, the frequency for  $N_j$   $\text{EPM}_j$  molecules reacting with the  $N_i$   $\text{EPM}_i$  molecules should be  $jN_j\bar{f}(\text{EPM}_i)$ . The total frequency ( $F_{i,j}$ ) for  $N_i$   $\text{EPM}_i$  molecules and  $N_j$   $\text{EPM}_j$  molecules reacting with each other will be assumed to be the sum of  $iN_i\bar{f}(\text{EPM}_j)$  and  $jN_j\bar{f}(\text{EPM}_i)$ . Using Eq. (18), we can now write

$$F_{i,j} = \frac{(-dN_{\text{CH}}/dt)(i+j) N_i N_j}{N_{\text{CA}}(0)N_{\text{CH}}(0)[\beta-1+N_{\text{CH}}/N_{\text{CH}}(0)]} = f_A(i+j) N_i N_j \quad (21)$$

where  $f_A = \frac{-dN_{\text{CH}}/dt}{N_{\text{CA}}(0)N_{\text{CH}}(0)[\beta-1+N_{\text{CH}}/N_{\text{CH}}(0)]}$ . It is obvious that  $F_{i,j} = F_{j,i}$ . Now we consider how  $N_n$  changes with reaction time. If an active site on  $\text{EPM}_n$  molecules reacts with an epoxy resin DGE B, the result is an increase in the length of an  $\text{EPM}_n$  molecule but  $N_n$  will not change.  $N_n$  changes only when the epoxy polymer molecules react with each other. The change in  $N_n$  consists of two parts: an increase in  $N_n$  when an  $\text{EPM}_i$  molecule reacts with an  $\text{EPM}_j$  molecule where  $(i+j) = n$  and a decrease in  $N_n$  when an  $\text{EPM}_n$  molecules reacts with any other epoxy polymer molecule. Based on the above conditions, we find the reaction rate to be

$$\frac{dN_1}{dt} = - \sum_{i=1}^{\infty} F_{1,i} = - \sum_{i=1}^{\infty} f_A (1+i) N_1 N_i \quad (22)$$

$$\frac{dN_2}{dt} = \frac{F_{1,1}}{2} - \sum_{i=1}^{\infty} F_{2,i} = f_A N_1 N_1 - \sum_{i=1}^{\infty} f_A (2+i) N_2 N_i \quad (23)$$

$$\begin{aligned} \frac{dN_3}{dt} &= F_{1,2} - \sum_{i=1}^{\infty} F_{3,i} \\ &= f_A(1+2)N_1N_2 - \sum_{i=1}^{\infty} f_A(3+i)N_3N_i \end{aligned} \tag{24}$$

.....

$$\begin{aligned} \frac{dN_n}{dt} &= \frac{1}{2} \sum_{i+j=n} F_{i,j} - \sum_{i=1}^{\infty} F_{n,i} \\ &= \frac{1}{2} \sum_{i+j=n} f_A(i+j)N_iN_j - \sum_{i=1}^{\infty} f_A(n+i)N_nN_i \end{aligned} \tag{25}$$

Let us compare Eq. (25) with the Smoluchowski coagulation equation<sup>74</sup>:

$$\frac{d\nu_n(t)}{dt} = \frac{1}{2} \sum_{i+j=n} K_{i,j} \nu_i \nu_j - \nu_n \sum_{i=1}^{\infty} K_{n,i} \nu_i \tag{26}$$

where  $K_{i,j}$  is the overall collection probability and  $\nu_n(t)$ , with  $n = 1, 2, \dots, \infty$ , is the concentration of  $n$ -size "droplets". The "droplets" could be any cluster of particles undergoing the coalescence process, e.g., cloud droplets, colloidal particles and so on. It is not difficult to see that Eq. (25) has the same form as Eq. (26) if we let  $f_A(i+j) = K_{i,j}$ . Eq. (26) has a known explicit solution<sup>75,76</sup> when the overall collection probability  $K_{i,j}$  is proportional to the sum of "droplet volumes" and is independent of time, i.e.  $K_{i,j} = b(i+j)$  with  $b$  being a constant. The pregelation solution is

$$\nu_n(t) = \nu_{\Sigma}(0) \frac{(\alpha n)^{n-1}}{n!} (1 - \alpha) e^{-\alpha n} \tag{27}$$

where  $\nu_{\Sigma}(0) = \sum_{n=1}^{\infty} \nu_n(0)$  and  $\alpha = 1 - e^{-\nu_{\Sigma}(0)bt}$ . For our copolymerization process, however, we cannot use Eq. (27) as the solution of Eq. (25) because  $f_A$  is not a constant with respect to time. We have to rearrange Eq. (25) since  $f_A$  is a function of the reaction time  $t$ . By using the definition of  $f_A$  and  $p$ , we can transform  $f_A dt$  as  $d\zeta$  by using the definitions of  $f_A$  after Eq. (21), where

$$\zeta = \frac{1}{N_{CA}(0)} \ln\left(\frac{1}{\beta - p}\right) \quad (28)$$

With Eq. (28), we rewrite Eq. (25) as

$$\frac{dN_n}{d\zeta} = \frac{1}{2} \sum_{i+j=n} (i+j) N_i N_j - \sum_{i=1}^{\infty} (n+i) N_n N_i \quad (29)$$

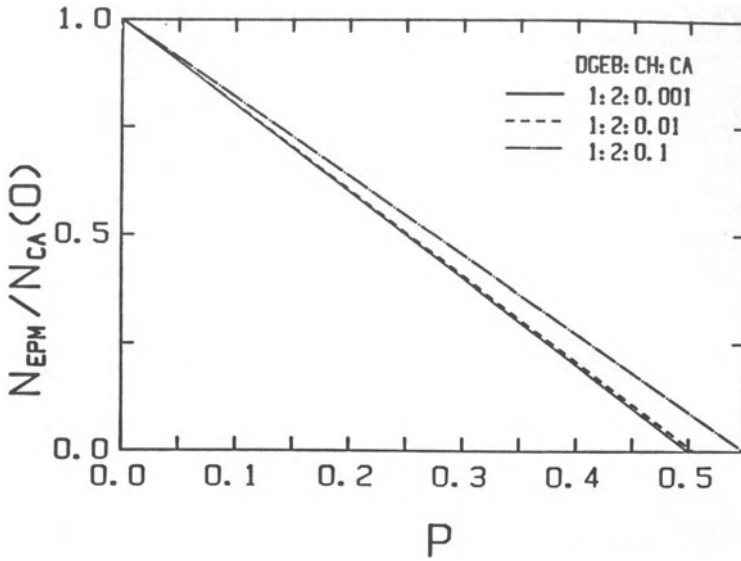


Figure 24. Plot of calculated total number of epoxy polymer molecules (EPM),  $N_{EPM}$ , normalized by initial number of catalyst molecules,  $N_{CH}(0)$ , versus the extent of conversion  $p$  ( $= 1 - N_{CH}(t)/N_{CH}(0)$ ) at different molar ratios of DGEb:CH:CA.

By comparing Eq. (29) with Eq. (26), we now have  $K_{i,j} = (i+j)$  and can apply the solution to Eq. (25), with  $b$  and  $\nu_{\Sigma}(0)$  replaced by 1 and  $N_{CA}(0)$ , respectively. Finally, we have the explicit solution to Eq.(25),

$$N_n(p) = N_{CA}(0) \frac{(\gamma p)^{n-1}}{n!} (1 - \gamma) e^{-\gamma p} \quad (30)$$

where  $\gamma = 1 - e^{-N_{CA}(0)[\zeta(p) - \zeta(0)]}$ . By using Eq. (28), we rewrite  $\gamma$  in the following form:

$$\gamma = \frac{pN_{CH}(0)}{N_{DGEb}(0) + N_{CA}(0)} = \frac{p}{\beta} \quad (31)$$

The total number of the epoxy polymer molecules ( $N_{EPM}$ ) should be  $\sum_{n=1}^{\infty} N_n(\zeta)$ , i.e.

$$N_{EPM} = \sum_{n=1}^{\infty} N_{CA}(0) \frac{(n\gamma)^{n-1}}{n!} (1 - \gamma)e^{-n\gamma} = N_{CA}(0)(1 - \gamma) \quad (32)$$

which is a linear function of the extent of conversion ( $p$ ). Figure 24 shows a plot of  $N_{EPM}/N_{CA}(0)$  as a function of  $p$  based on Eq. (32) for the molar ratios of DGEb:CH:CA = 1:2:0.001, 1:2:0.01 and 1:2:0.1, respectively. From Eq. (30), we can calculate  $N_n$  and the number distribution  $f_N(EPM_n)$  with different extents of conversion ( $p$ ) for the copolymerization reaction. Figure 25 shows a plot of  $f_N(EPM_n)$  versus the number ( $n$ ) of active sites on the  $EPM_n$  molecule for the same molar ratios of DGEb:CH:CA in Fig. 24 at different  $p$  values with  $p = 0.1, 0.2, 0.3, 0.4$  and  $0.45$ , respectively. Figure 26 graphically shows how  $N_n$  changes with  $p$  for the same molar ratios of DGEb:CH:CA in Fig. 24. From Figure 26, we note that there is a maximum number of molecules for every type of  $EPM_n$  molecule during the copolymerization process. The location

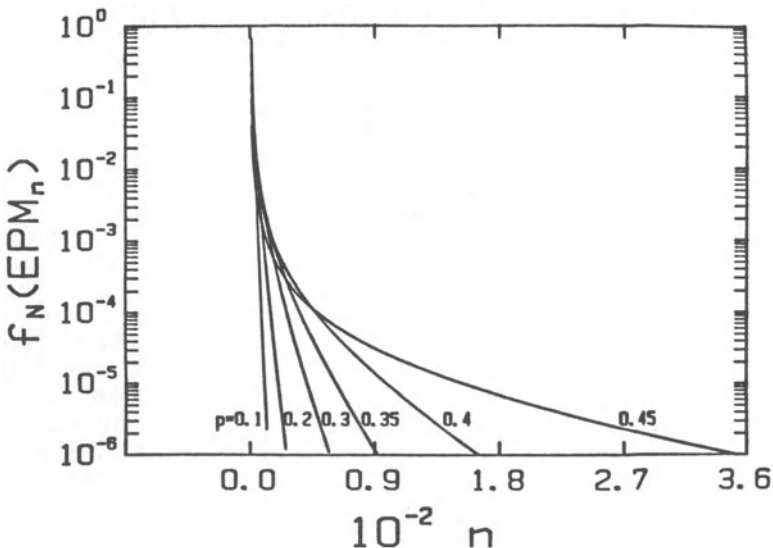


Figure 25. Plot of calculated number of epoxy polymer molecules with  $n$  branching points ( $N_n$ ) versus  $n$  at different conversion extent ( $p$ ) for the same molar ratios as in Fig. 24.

of  $p_{\max}(n)$  can be calculated by letting  $dN_n/dp = 0$ . The result is that

$$p_{\max}(n) = \beta \left[ 1 - \left( \frac{1}{n} \right)^{1/2} \right] \quad (33)$$

When  $n = 1$ ,  $p_{\max}(1) = 0$ . This is appropriate because  $N_1$  always decreases as the reaction proceeds. When  $n \rightarrow \infty$ ,  $p_{\max}(\infty) \rightarrow \beta$ . This behavior can be seen in Fig. 26.

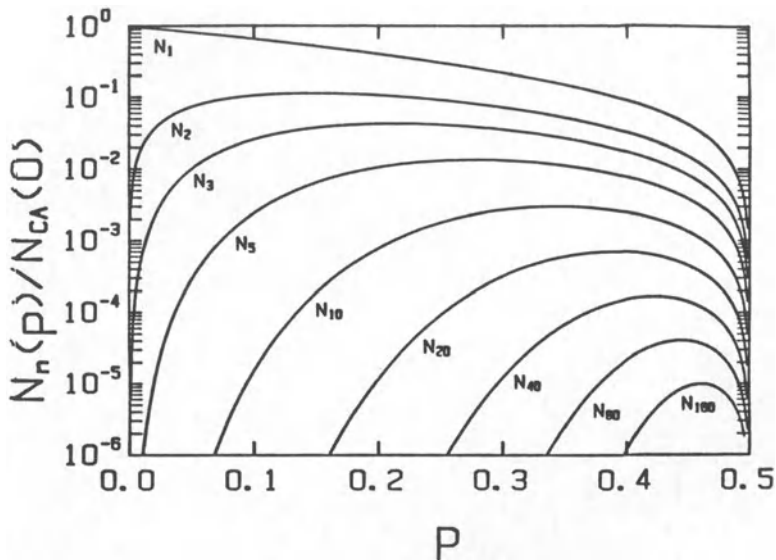


Figure 26. Plot of calculated number of epoxy polymer molecules with  $n$  branching points ( $N_n$ ) versus  $p$  for different values of  $n$  but the same molar ratios as in Fig. 24.

By means of chemical analysis,<sup>30</sup> we monitored the extent of CH conversion during the copolymerization reaction. As the reaction approaches its gelation threshold, the chemical analysis becomes more and more difficult and inaccurate because the reaction mixture becomes very viscous and more gel-like. Experimentally, we defined the gelation threshold by constantly taking out the reaction mixture from the reaction vessel and dissolving it in MEK during the curing process until

the moment when we observed a trace amount of undissolved epoxy polymers appearing in the solution. The extent of conversion corresponding to that moment is defined as the critical conversion extent ( $p_c$ ). We defined that moment as the gelation threshold. Theoretically, the gelation threshold can be defined as the point at which all epoxy polymer molecules are linked to each other to form an infinite network. This means that  $N_{EPM} = 1$  at the gelation threshold. Our definition on the gelation threshold is somewhat different from what has been defined in the past. Based on the definition that the critical conversion extent ( $p_c$ ) is the point at which the branching probability of the reaction is equal to the non-branching probability of the reaction. The gelation threshold should occur earlier than  $p_c$  according to our definition. Our experimental observation has indeed shown that the gelation threshold occurs before  $N_{EPM} = 1$ , i.e., the entire system becomes one giant polymer. By using Eq. (15) and the above definition, we can calculate that  $p_c = \beta$ . Both the experimentally determined  $p_c$  (expressed as hollow squares) and the calculated  $p_c$  (expressed as hollow triangles) for the molar ratio of DGEb:CH = 1:2 but different amounts of CA are plotted in

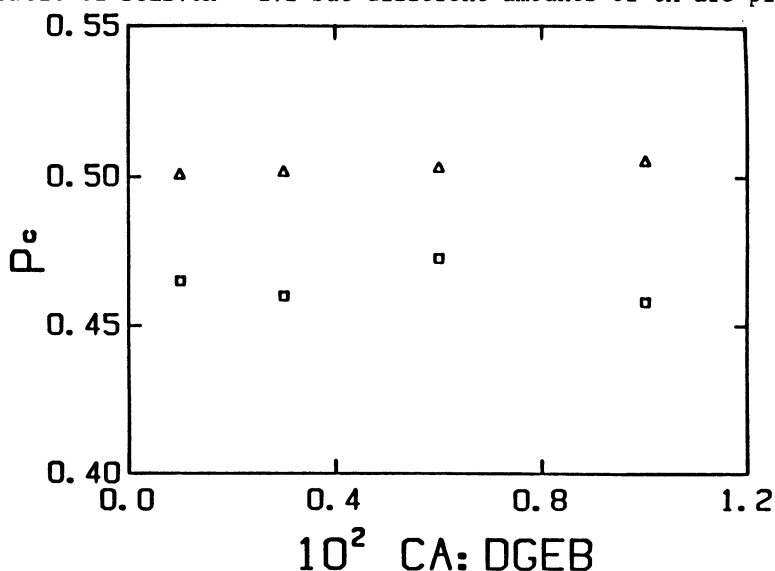


Figure 27. Plot of measured and calculated critical conversion extent ( $p_c$ ) versus different molar ratios of CA:DGEb, but keeping DGEb:CH = 1:2 and 80°C. (Reproduction of Fig. 5 of Ref. 82)

Fig. 27. The experimental results show that  $p_c$  is essentially constant, independent of the molar ratio variations in CA:DGEb from 0.001 to 0.01, as predicted by the calculated results. We also observed that the

experimentally determined  $p_c$  values were about 7% smaller than the calculated values. The difference existed systematically for all four different catalyst concentrations. There could be two possible reasons for this systematic deviation. (i) Our experimental criteria for  $p_c$ , i.e. the solubility test and the rate of light scattering intensity change, is not the same as the theoretical one. At the experimental  $p_c$ , the copolymerization process has not yet reached the stage of an infinite network, which is the criterion according to theory. (ii) As the reaction approaches the gelation threshold, some or all of the assumptions for the proposed branching kinetics break down, especially, the formation of rings inside highly branched epoxy polymers. The rings could produce a finite macro-size three dimensional network as evidenced by the insoluble gel particles. If we assume that  $f_A$  appearing in Eq. (21) is independent of reaction temperature, then the theoretical  $p_c$  ( $=\beta$ ) yields a gelation threshold that is also independent of reaction temperature. Figure 28 shows a plot of the experimentally determined  $p_c$  values as a function of reaction temperature. The reaction temperature has indeed only a weak effect on the gelation threshold in terms of the extent of conversion.

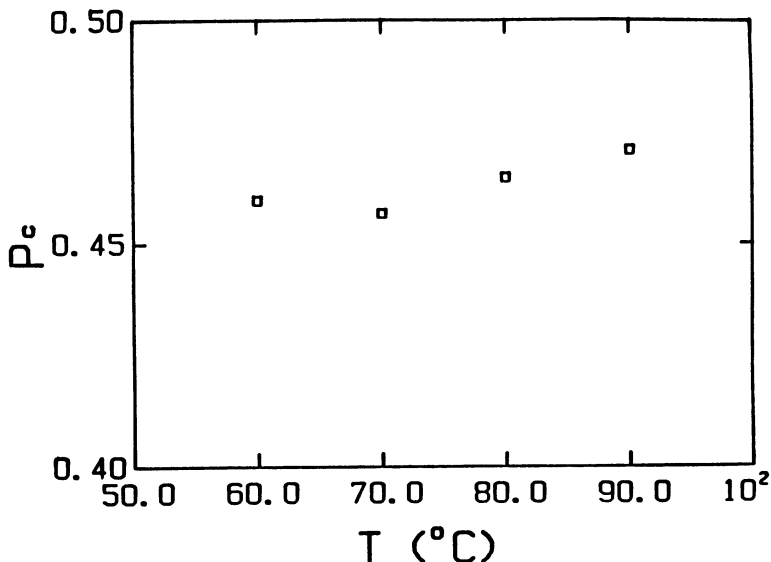


Figure 28. Plot of measured critical conversion extent ( $p_c$ ) versus the reaction temperature ( $T$ ) for the reaction mixture at the molar ratio of DGEb:CH:CA = 1:2:0.001. (Reproduction of Fig. 6 of Ref. 82)

By assuming that all catalyst molecules start the polymerization reaction at the same time, each active site grows at the same speed and produces the same linear length ( $l_0$ ) of the subpolymer chain. The molecular weight for the subpolymer chain ( $l_0$ ), denoted as  $M(l_0)$ , should be the total reacted weight divided by the number of active sites (i.e.  $N_{CA}(0)$ ).

$$M(l_0) = \frac{p N_{CH}(0) (M_{DGEb} + M_{CH})}{N_{CA}(0)} + M_{CA} \quad (34)$$

where  $M_{DGEb}$ ,  $M_{CH}$  and  $M_{CA}$  are the molecular weight of DGEb, CH and CA, respectively. In this way, each  $EMP_n$  molecule has  $n$  such subpolymer chains. The molecular weight for  $EPM_n$  molecule should be  $n$  times  $M(l_0)$ , i.e.  $M(EPM_n) = nM(l_0)$  which represents a consequence of our stringent assumptions. Together with Eq. (34), the number-average molecular weight ( $M_n$ ) at different  $p$  can be written as

$$M_n = \frac{\sum_{n=1}^{\infty} M(EPM_n) N_n}{\sum_{n=1}^{\infty} N_n} = \frac{M(l_0) \sum_{n=1}^{\infty} n N_n}{\sum_{n=1}^{\infty} N_n} = \frac{M(l_0)}{(1 - \gamma)} \quad (35)$$

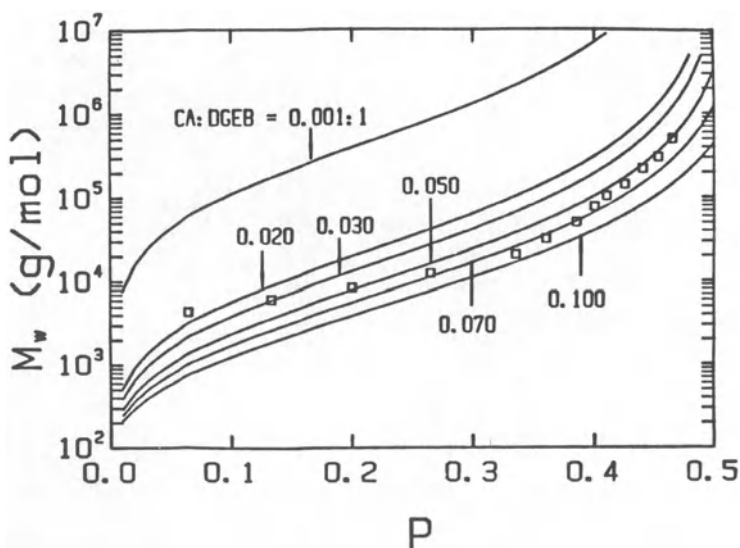


Figure 29. Plot of calculated  $M_w$  versus  $p$  for fixed molar ratio of

DGEB:CH = 1:2 but different amount of catalyst CA. Measured  $M_w$  versus  $p$  for the molar ratio of DGEB:CH:CA = 1:2:0.001 at 80°C are also plotted in the Figure. (Reproduction of Fig. 7 of Ref. 82)

and the weight-average molecular weight ( $M_w$ ),

$$M_w = \frac{\sum_{n=1}^{\infty} M(EPM)_n f_w(M)}{\sum_{n=1}^{\infty} f_w(M)} = M(l_o) \sum_{n=1}^{\infty} n^2 N_n = M(l_o) \left( \frac{1}{1-\gamma} \right)^2 \quad (36)$$

Figure 29 shows how calculated  $M_w$  changes with the extent of conversion  $p$  at a fixed molar ratio of DGEB:CH = 1:2 but different amounts of catalyst CA. The measured  $M_w$  versus  $p$  for the reaction mixture at a

fixed molar ratio of DGEB:CH:CA = 1:2:0.001 at 80°C are also plotted in Figure 29. By comparison, we find that the assumptions about no termination for the active site and no catalyst transfer during the reaction process are too stringent. There is not a single calculated curve which fits the measured data over the entire measured range of  $p$ . In the actual copolymerization reaction, the catalyst molecules are transferred constantly to form new active sites.<sup>73</sup> This means that the reaction mixture would actually have more active sites than the number of catalyst molecules. Then the number of active sites become a function of reaction time. In Fig. 29, by varying the molar ratio of catalyst CA to DGEB in the calculation, we have simulated the catalyst transfer

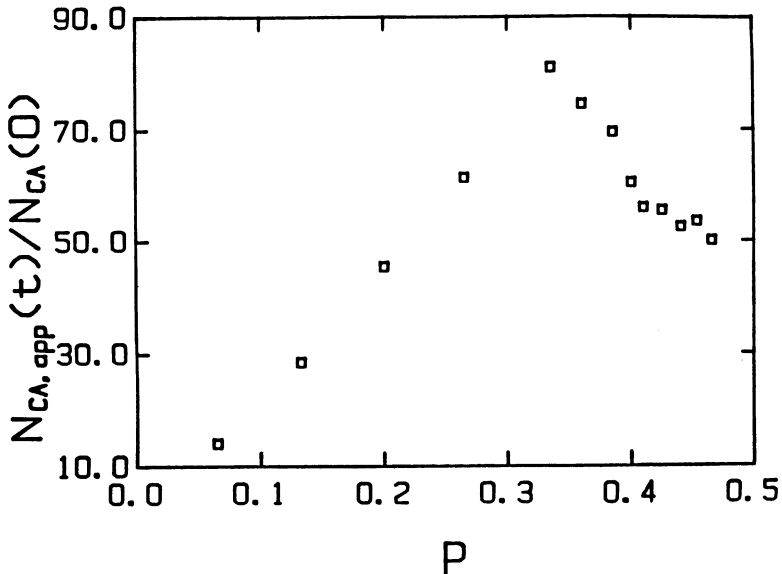


Figure 30. Plot of simulated  $N_{CA,app}^{(0)}/N_{CA}^{(0)}$  versus  $p$  at a fixed molar ratio of DGEb:CH = 1:2 and  $80^{\circ}\text{C}$ , where the  $N_{CA,app}^{(t)}$  is the apparent total active sites in the reaction mixture at reaction time  $t$ .

during the copolymerization process for the real reaction. Thus, by comparing the calculated curves with the experimental data points, we have obtained information about how many times the catalyst molecules are transferred to form new active sites during the reaction process. The apparent number of active sites in the reaction mixture at time  $t$  is denoted as  $N_{CA,app}^{(t)}$ .  $N_{CA,app}^{(t)}/N_{CA}^{(t=0)}$ , which corresponds to the average number of times each catalyst molecule has been transferred to form new active sites at reaction time  $t$ , versus the extent of conversion ( $p$ ) are plotted in Figure 30. In Fig. 30, we can see that the average number of times a catalyst molecule is being transferred is a linear function of the extent of conversion. The apparent number of the active sites is about 15 times greater than  $N_{CA}^{(t=0)}$  at  $p = 0.07$  and about 80 times greater at  $p = 0.35$ . The same phenomena was observed by Fischer.<sup>73</sup> We also observed that the amount of active sites decreases for  $p > 0.35$ . Why should there be a decrease in the number of active sites in the copolymerization reaction for  $p > 0.35$ ? We know that the viscosity of the reaction mixture increases as the extent of conversion increases and the epoxy polymer molecules become larger and larger. Some active sites inside the larger polymer molecules will have less chance to react with other polymer molecules. The larger polymer molecules move at lower speeds than the smaller molecules implying that effectively the active sites on the larger polymer molecules have less activity than

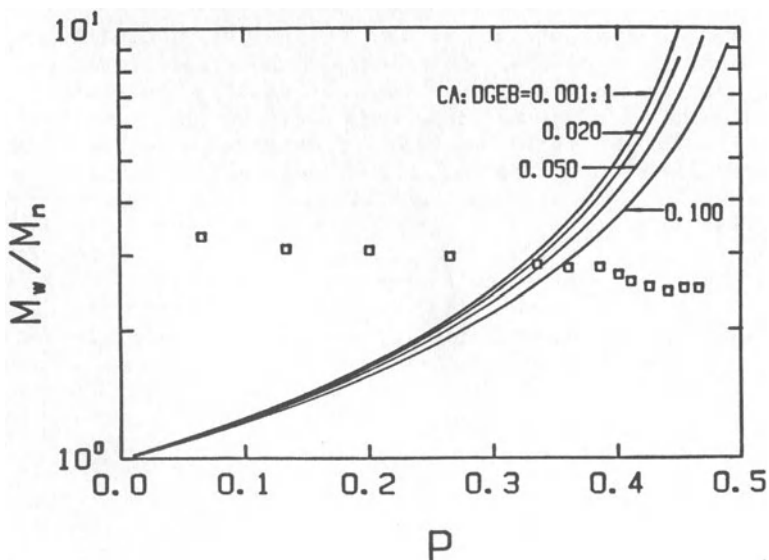


Figure 31. Plot of calculated ratio of the weight-average molecular weight to the number-average molecular weight ( $M_w/M_n$ ) versus  $p$  for a fixed molar ratio of DGEb:CH = 1:2 but different amounts of catalyst CA. Measured  $M_w/M_n$  versus  $p$  for the molar ratio of DGEb:CH:CA = 1:2:0.001 at 80°C are also shown in Figure 31. (Reproduction of Fig. 9 of Ref. 82)

those on the smaller polymer molecules. Figure 31 shows that calculated ratio of  $M_w/M_n$  ( $= \frac{1}{1-\gamma}$ ) versus  $p$  at a fixed molar ratio of DGEb:CH = 1:2 but different amounts of catalyst CA. The measured  $M_w/M_n$  values, denoted by hollow squares in Fig. 31, are completely different from the theoretical prediction. At low conversion extent, the calculated  $M_w/M_n$  values are much smaller than the measured values. At higher conversion extent, this relation is reversed. The difference can be explained as follows. At low conversion extent, the calculation assumes that the starting molecules are monodisperse, i.e.  $M_w/M_n = 1$ . For the real reaction, the epoxy polymer is already polydisperse when the branching process starts. At high conversion extent, there are not only very larger branched polymer molecules in the reaction mixture, but also very small epoxy polymer molecules, confirming a high polydispersity index. In light scattering, the presence of larger particles are emphasized, resulting in smaller measured  $M_w/M_n$  values for highly polydispersed systems with large amounts of smaller particles. The use of size-exclusion chromatography together with light scattering for analysis of branched epoxy polymer is underway.

The deviations of the calculated  $M_w$  and  $M_w/M_n$  with the measured ones as shown in Figures 29 and 31, respectively, clearly suggests a need for modification of the assumptions in the theoretical development, especially on assumption (1), i.e., all catalyst molecules start the polymerization reaction at the same time and have the same reactivity, and they will not be terminated or transferred. We have considered possible breakdowns on the transfer and termination of active sites. More importantly, from our experimental observation, we have noted that the molecular weight distribution of the epoxy polymer formed is polydisperse even in the very early reaction stages. Thus, the assumption that the catalyst molecules start the polymerization reaction at the same time must not be valid. We now modify our theory by assuming a simple Gaussian-like distribution on the number of EPM<sub>n</sub> formed at some initial extent of conversion  $p_0$ .

$$N_n(p_0) = \frac{N_{EPM}(p_0)}{\bar{n}(p_0)} \exp\left(-\frac{n}{\bar{n}(p_0)}\right) \quad (37)$$

where  $N_{EPM}(p_0)$  and  $\bar{n}(p_0)$  are the total number of epoxy polymer molecules at  $p_0$  and the mean active site per epoxy polymer molecule at  $p_0$ . For this particular type of initial condition, Golovin<sup>75</sup> and Scott<sup>76,77,78</sup> have shown that Eq. (29) can be solved by using Laplace transforms and a conformal transformation, yielding an exact solution

$$N_n(p) = \left(1 - \frac{p-p_0}{\beta-p_0}\right) \exp\left[-\left(\frac{p-p_0}{\beta-p_0}+1\right)\frac{n}{\bar{n}(p_0)}\right] \sum_{m=0}^{\infty} \frac{\left(\frac{p-p_0}{\beta-p_0}\right)^m [n/\bar{n}(p_0)]^{2m}}{(m+1)!m!} \quad (38)$$

By combining Eq. (38) with Eq. (36), we are able to calculate  $f_w(M)$  at different conversion  $p$ . The calculated results are shown in Figure 3:

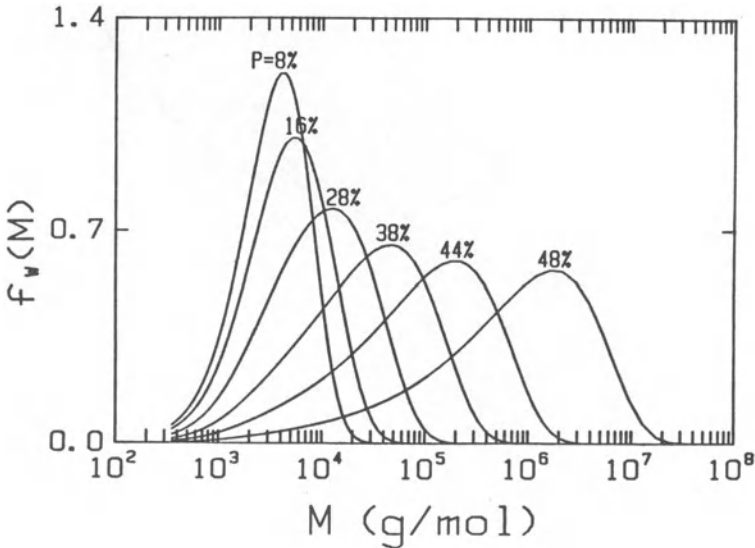


Figure 32. Plot of calculated weight distribution ( $f_w(M)$ ) versus  $M$  at different extent of conversion  $p$  by using Eq. (38) where  $p_0 = 0.065$ ,  $\bar{n}(p_0) = 1$ , and DGEb:CH:CA = 1:2:0.001. (Reproduction of Fig. 10 of Ref. 82)

where we have chosen  $M_w = 4.1 \times 10^3$  (g/mol) at  $p_0 = 0.065$ , which is the lowest experimentally measured molecular weight as shown in Figure 29. In Figure 32, we see that the molecular weight distribution is spreading as the reaction approaches the gelation threshold. The long low molecular weight tails obviously give a much higher theoretical value of  $M_w/M_n$  than the measured ones because laser light scattering tends to emphasized higher molecular weight fractions. From the calculated  $f_w(M)$ , we can further compute out the weight-average molecular weight  $M_w$  at each reaction stage. The solid line in Figure 33 represents the calculated  $M_w$  values based on  $f_w(M)$  values in Figure 31, and the hollow squares are the same experimental data as shown in Figure 29. Figure 33 shows that the agreement between the calculated curve and measured  $M_w$  values is fairly good. It suggests that the introduction of Eq. (37) has provided a realistic approach to using the Smoluchowski coagulation equation for epoxy polymerization studies.

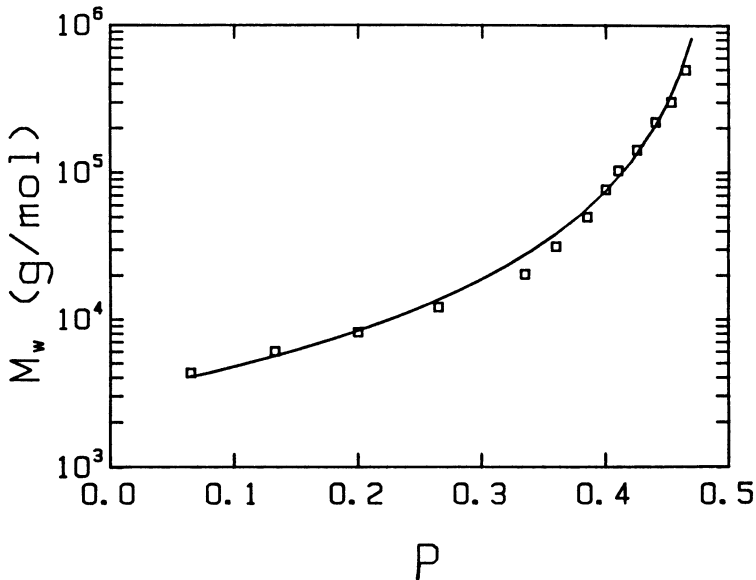


Figure 33. Plot of weight-average molecular weight  $M_w$  versus  $p$ . Solid

line represents the calculated values by using Eq. (25) where  $p_o = 0.065$ ,  $\bar{n}(p_o) = 1$ , and DGEb:CH:CA = 1:2:0.001. Hollow squares show the real experimental data with the same ratio of DGEb:CH:CA at 80°C. (Reproduction of Fig. 9 of Ref. 82)

### 3.7. Study of LLS envelope of Epoxy polymers

Debye and Bueche<sup>29</sup> proposed that the intensity of scattered light (i) of an inhomogeneous solid follows the expression:

$$i \propto 4\pi\eta^2 V \int_0^\infty r^2 \gamma(r) \frac{\sin(Kr)}{Kr} dr \quad (39)$$

where  $V$  is the scattering volume,  $\eta^2$  is the mean square average local dielectric constant fluctuations, and  $\gamma(r)$  is a correlation function defined by

$$\gamma(r) = \langle \eta_1 \eta_2 \rangle / \eta^2 \quad (40)$$

where  $\eta_1$  and  $\eta_2$  are the local dielectric constant fluctuations in volume elements 1 and 2, respectively. For all pairs of volume elements separated by a scalar distance  $r$  inside the scattering volume,  $\langle \eta_1 \eta_2 \rangle$  is the average value of  $\eta_1 \eta_2$ . If we take the correlation to be random,

$$\gamma(r) = e^{-r/a} \quad (41)$$

where  $a$  is the correlation length defining the local inhomogeneities. The Rayleigh ratio for unit scattering volume has the form

$$R_{vv}(K) = \frac{8\pi^3 \eta^2 a^3}{\lambda_o^4 (1+K^2 a^2)^2} \quad (42)$$

We could calculate  $a$  and  $\eta^2$  from the Rayleigh ratio by plotting  $(R_{vv}(K))^{-1/2}$  versus  $K^2$ .

$R_{vv}(K)_{K=0}$  at a fixed catalyst concentration (0.1%) changes with reaction time at four different temperatures. In order to find the temperature effect, we rescaled the reaction time at each temperature by

multiplying it with the corresponding  $k_0$  value. The results are shown in

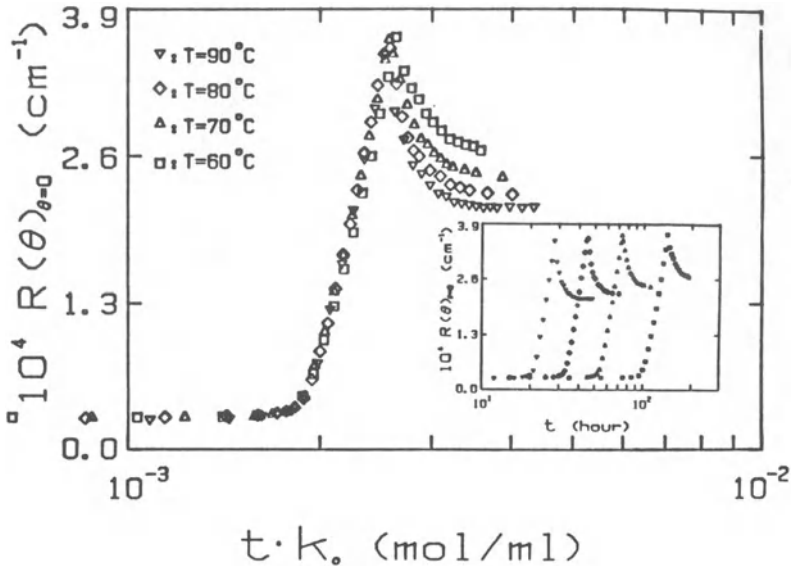


Figure 34.  $R_{\text{VV}}(\theta)_{\theta=0}$  versus scaled reaction time,  $k_0 t$  (in units of mole/mL), at four different reaction temperatures,  $60^\circ\text{C}$ ,  $70^\circ\text{C}$ ,  $80^\circ\text{C}$  and  $90^\circ\text{C}$ . The molar ratio of DGEb:CH:CA = 1:2:0.001. Inset: Unscaled  $R_{\text{VV}}(\theta)_{\theta=0}$  versus reaction time  $t$  (in units of hour). (Reproduction of Fig. 3 of Ref. 81)

Figure 34. We note that the temperature has little effects on  $R_{\text{VV}}(K)_{K=0}$  before  $R_{\text{VV}}(K)_{K=0}$  reaches its maximum value. After having passed the maximum,  $R_{\text{VV}}(K)_{K=0}$  tends to behave differently at different temperatures. The higher the reaction temperature, the smaller the value of  $R_{\text{VV}}(K)_{K=0}$  becomes. The phenomenon is reasonable because the system becomes more uniform and scatters less light at higher reaction temperatures. A similar phenomenon was observed when we changed the catalyst concentration, i.e., the higher the catalyst concentration, the more uniform the reaction mixture becomes and the less the scattered intensity. The optical behavior tells us that the polymerization reaction produced essentially the same degree of local dielectric constant fluctuations as long as the catalyst concentration is greater than a threshold value (say  $\approx 0.3\%$ ). From the light scattering intensity studies on in situ epoxy reaction mixtures, we can make the following observations:

(1) The higher the temperature, the smaller the  $\eta^{-2}$  value and the larger the extension of local inhomogeneities, in terms of  $a$ .

(2) The lower the catalyst concentration, the smaller the  $\eta^{-2}$  values and the larger the extension of local optical inhomogeneities. This observation suggests that at lower catalyst concentrations each polymer molecule has more chance to grow bigger before it reacts with other polymer molecules.

(3) There are two different rates associated with the characteristic length increases with time. After having reached its maximum value (around 70 nm), the correlation length  $a$  gradually decreases to a constant value at around 60 nm. The changes in the  $\eta^{-2}$  values also show three main steps: a sharp drop, a gradual increase, and then a steady state. Each crossover point on the  $\eta^{-2}$  values corresponds to a change of behavior on the average characteristic length of local inhomogeneities.

By combining this observation with the knowledge we gained before, we propose that the reaction process can be divided into four main

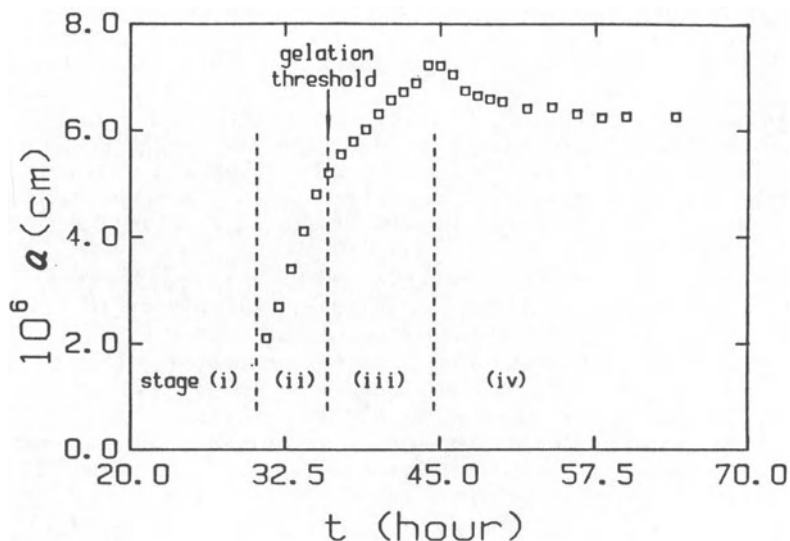


Figure 35. Correlation length ( $a$ ) of local optical inhomogeneities versus reaction time  $t$  at  $80^\circ\text{C}$ . Catalyst concentrations is 0.1% and the molar ratio of DGEb:CH = 1:2. (Reproduction of Fig. 7 of Ref. 81)

regions. It is shown in Figure 35. (i) In the very beginning, the size of inhomogeneities is too small to be observed by laser light

scattering. Most of the initial polymer product are linear or slightly branched polymer molecules. The growth of the polymer chains in this first stage is accompanied mainly by the reaction of the epoxy monomers with the curing agent. There is a gradual increase in the size of inhomogeneities through the growth of polymer molecules with some crosslinking. At the same time, the optical density difference between the polymer chains and the reaction mixture becomes larger as the

polymer size becomes larger. The  $\bar{\eta}^2$  value must gradually increase to its maximum value until crosslinking dominates the copolymerization reaction. In the above discussion, we have assumed that polymers are formed only at the catalytic centers and therefore, there is no increase in polymer number concentration. With increasing extent of conversion, the concentration of lower molecular weight polymers whose refractive index increment has reached a plateau value becomes higher and higher. Then the system enters the second stage. (ii) In the second stage, the polymer molecules have more chance to react with each other to form larger and more highly branched polymer molecules. It is easy to understand that the characteristic size of inhomogeneities increases very fast because the polymer chains almost double themselves in size by covalent bonding among the polymer chains. We also notice that the values of  $\bar{\eta}^2$  decrease by a factor of about two. How do we interpret this

observation? Let us look at the definition of  $\bar{\eta}^2$ .  $\eta$  is a local variation of the dielectric constant superimposed on the average dielectric constant  $\epsilon$ . In the second stage when the polymer molecules have overlapped to form local polymer networks, the amount of polymer per unit volume is increasing, but the crosslinked polymer networks tend

to shrink in size. So, the relative values of  $\bar{\eta}^2$  decrease. As the polymer molecules become bigger and bigger, all polymer molecule inside the network will tend to become more connected with one other. Then, the gel state has fewer and fewer loose polymer molecules not connected with the network. (iii) In third stage, most of the polymer chains cannot move freely and the viscosity of the system becomes higher, i.e. the polymer chains are localized. Direct reaction between polymer chains becomes more difficult, but the monomers (and small polymer chains) are still moving around to react with the localized larger polymer chains. The extent of local optical inhomogeneities increases at a lower rate. At the same time, the localized polymerization reaction densifies the branched polymer chains, and thus increasing the contrast of the polymer domain to the average background of the system. However, this increase

is limited, as shown by a small increase in  $\bar{\eta}^2$  value during the third stage. We suggest that the crossover point for the average size of local optical inhomogeneities from one rate to another, or the lowest value of

$\bar{\eta}^2$ , could be considered as the gel point, which we marked out in Figure 35. (iv) In the final stage, the unreacted monomers still move inside

the system to react with the crosslinked polymer chains. Experimentally we observed that the size of local optical inhomogeneities reduced to a constant value and  $\eta^{-2}$  values remained unchanged. This observation suggests that light scattering observes different sources of local optical inhomogeneities.

#### 4. CONCLUSIONS

Branched polymer structures and macromolecular properties of epoxy polymers in solution can be investigated using a combination of scattering techniques. By combining laser light scattering with small angle x-ray scattering, we have developed a methodology to determine the molecular weight and the molecular weight distribution of random polymer structures before its gelation threshold during the curing process. Our method differs from the usual analytical technique such as size exclusion chromatography because we do not require fractionation of random branched polymers in solution but take advantage of the fractal geometry of random structures which can be determined by SAXS. By using the LLS approach described in this article, we can study how temperature, composition and catalyst effect the epoxy polymerization process and determine the molecular weight distribution at different reaction stages without relying on the more tedious analytical technique of size exclusion chromatography. Experimentally, we have further shown that there exists a scaling relationship for the molecular weight distribution in the sol phase of the crosslinked epoxy-anhydride system. The scaling constant  $\tau$  ( $= 2.1 \pm 0.1$ ) is very close to our previously determined fractal dimension  $d_f$  ( $= 2.17 \pm 0.05$ ).

The Debye-Bueche theory for inhomogeneous solids has been applied to studies of the formation of polymer networks in an epoxy polymerization reaction. As an on-line technique, laser light scattering has a unique advantage, capable of monitoring the local optical inhomogeneities during the curing process. Based on our experimental data, four main reaction stages are proposed. By combining our results with other measurements about the mechanical properties of the system, we may be able to establish a relationship between the microstructure and macroscopic properties of the cured epoxy resins. Finally, light scattering could also be used to estimate the gel point in optically clear epoxy resins.

A simplified model is proposed for the branching kinetics of the epoxy resin (DGEb) cured with the anhydride (CH) in the presence of the triamine (CA) as a catalyst. We show, for the first time, that the branching kinetics can be approximated by using the Smoluchowski coagulation equation. In a simple version of that equation used here, the overall branching probability has been taken as proportional to the sum of active sites on the two polymers. The calculated weight-average molecular weight based on the model using two different initial conditions, i.e., monodisperse polymer at  $p_0 = 0$  and polydisperse

polymer at  $p_0 = 0.065$  as observed experimentally and the measured weight-average molecular weight as a function of  $p$  have been compared. The results show that the initial molecular weight distribution is not uniform. By using a Gaussian-like distribution, we can predict the nature of the epoxy polymer product from knowledge in the early stage of the polymerization process. The model also implies that the catalyst molecules do not start the reaction at the same time. Dusek et al<sup>79</sup> have discussed a statistical branching theory in an analysis of gelation of a similar system, diepoxide-cyclic anhydride-tert.-amine. However, their emphasis was mainly on the critical extent of conversion at the gelation threshold. The measured polydisperse index ( $M_w/M_n$ ) does not agree with the calculated one because laser light scattering emphasizes larger particles. We have to use the other techniques to measure the low molecular weight tails in the distribution in order to provide a more detail test of the model. A more general form for the reaction kernel and other forms of the initial distribution should be considered. Further experimental and theoretical studies are underway.

Finally, in my lecture review of our recent epoxy works,<sup>32,61,80-82</sup> I should mention that Dr. Chi Wu has been the main driving force from experiments to theory and support of this project by the U.S. Army Research Office is gratefully acknowledged.

## References

1. See for example, Antoon, M. K. and Koenig, J. L., J. Polym. Sci. Polym. Chem. Ed. 1981, 19, 549, and references therein.
2. D. A. Weitz and M. Y. Lin, Phys. Rev. Lett., 1986, 57, 2037.
3. R. C. Ball, D. A. Weitz, T. A. Witten and F. Leyvraz, Phys. Rev. Lett. 1987, 58, 274.
4. P. G. J. van Dongen and M. H. Ernst, J. Phys. A: Math. Gen., 1985, 18, 2779.
5. P. G. J. van Dongen and M. H. Ernst, Phys. Rev. Lett., 1985, 54, 1396.
6. M. Kolb, Phys. Rev. Lett., 1984, 53, 1653.
7. R. Botet and R. Jullien, J. Phys. A, 1984, 17, 2517.
8. F. Leyvraz, Phys. Rev. A, 1984, 29, 854.
9. M. H. Ernst, E. M. Hendriks and R. M. Ziff, J. Phys. A: Math. Gen., 1982, 15, L743.
10. M. H. Ernst, E. M. Hendriks and R. M. Ziff, Phys. Lett., 1982, 92A, 267
11. R. M. Ziff and G. Stell, J. Chem. Phys., 1980, 73, 3492.
12. Mandelbrot, B.B. "Fractals, Form, Chance and Dimension," Freeman, San Francisco, 1977; "The Fractal Geometry of Nature," Freeman, New York, 1982.
13. Stanley, H.; Reynolds, P.; Redner, S; Family, F. in Real Space Renormalization; Burkhardt, T.W.; van Leeuwen, J.M.J., Eds.; Springer: New York, 1982, Chap. 7.
14. Schaefer, D.W.; Martin, J.E.; Wiltzius, P.; Cannell, D.S. Phys. Rev. Lett. 1984, 52, 2371.
15. Martin, J.E.; Schaefer, D.W. Phys. Rev. Lett. 1984, 53, 2457.
16. Wiltzius, P. Phys. Rev. Lett. 1987, 58, 710.
17. Schaefer, D.W.; Keefer, K.D. Phys. Rev. Lett. 1984, 53, 1383.
18. Chambon, F.; Winter, H.H. Polym. Bull. (Berlin) 1985, 13, 499.
19. Muthukumar, M.; Winter, H.H. Macromolecules 1986, 19, 1284.
20. Feder, J.; Jossang, T. Phys. Rev. Lett. 1984, 53, 1403.
21. Weitz, D.A.; Huang, J.S.; Lin, M.Y.; Sung, J. Phys. Rev. Lett. 1985, 54, 416.
22. Witten, T.A.; Sander. L.M. Phys. Rev. Lett. 1981 47, 1400.
23. Meakin, P. Phys. Rev. Lett.A 1983, 27, 604, 1495.
24. Kaufman, J.H.; Baker, C.K.; Nazzari, A.I.; Flickner, M.; Melroy, O.R. Phys. Rev. Lett. 1986, 56, 1932.
25. Family, F. in Random Walks and Their Applications in the Physics and Biophysical Sciences - 1982; Schlesinger, M.F., West, B.J., Eds.; AIP Conference Proceedings No. 109; Amer. Inst. Phys.: New York, 1984, p.33.
26. Meakin, P. Phys. Rev. Lett. 1983, 51, 1119.
27. Kolb, M.; Botet, R.; Jullien, J. Phys. Rev. Lett. 1983, 51, 1123.
28. Hentschel, H.G.E.; Deutch, J.M. Phys. Rev. Lett.A 1984, 29, 1609.
29. Debye, P. and Bueche, A. M., J. Appl. Phys., 1949, 20, 518
30. May, C. A. and Tanaka Y. Epoxy Resins Chemistry and Technology; Marcel Dekker: New York, 1973; p 683.

31. Chu, B. and Wu, C., Macromolecules, 1987, 20, 93.
32. Chu, B., Wu, C., Wu, D.-Q. and Phillips, J. C., Macromolecules, 1987, 20, 2642.
33. Kratky, O. and Oelschlaeger, H. J. Coll. & Interface Sci. 1969, 31, 490.
34. Sander, L.M. Nature, 1986, 322, 789; Scientific American 1986, 256, 94.
35. Meakin, P. "Fractal Aggregates and Thin Fractal Measures," to be published. See references therein.
36. Stanley, H.E. J. Phys. 1977, A10, L211.
37. Cotton, J.P. J. Physique Lett. 1980, 41, 231.
38. Daoud, M.; Family, F.; Jannink, G. J. Phys. Lett. 1984, 45, 199.
39. Schosseler, F.; Leibler, L. Macromolecules 1985, 18, 399.
40. Leibler, L.; Schosseler, F. Phys. Rev. Lett. 1985, 55, 1110.
41. Martin, J.E.; Ackerson, B.J. Phys. Rev. A, 1985, 31, 1180.
42. Bouchard, E.; Delsanti, M.; Adam, M.; Daoud, M.; Durand, D. J. Physique, 1986, 47, 1273.
43. Mandelbrot, B.B. in "Fractals in Physics," Proceedings of the 6th International Symposium of ICTP, L. Pietronero and E. Tosatti, eds., North Holland, Amsterdam, 1986, p. 3,17 and 21.
44. Daoud, M.; Joanny, J.F. J. Physique 1981, 42, 1359.
45. Huber, K.; Burchard, W.; Fetters, L.J. Macromolecules 1984, 17, 541.
46. See "Proceedings of the 5th International Conference on Photon Correlation Techniques in Fluid Mechanics," Springer Series in Optical Sciences (Ed. E.O. Schulz-DuBois) Springer-Verlag, New York, 1983.
47. Chu, B., Ford, J. R. and Dhadwal, H.S., in "Methods of Enzymology", (Eds. S.P. Colowick and N.O. Kaplan) Academic Press, Inc., Orlando, Florida, Vol. 117, 1985, pp. 256-297.
48. Chu, B., Ying, Q.-C., Wu, C., Ford, J. R. and Dhadwal, H. S. Polymer, 1985, 26, 1408.
49. Wu, C., Buck, W. and Chu, B., Macromolecules, 1987, 20, 98.
50. Chu, B., Wu, C. and Buck, W., Macromolecules, 1989, 22 (No. 2) 831
51. Grubisic, Z., Rempp, P. and Benoit, H., J. Polym. Sci., Part B, 1967, 5, 753-759.
52. Moore, J. C. and Hendrickson, J. G., J. Polym. Sci., Part C, 1965, 8, 233-241.
53. Mori, S., J. Chromatogr., 1978, 157, 75-84.
54. Mori, S., J. Appl. Polym. Sci., 1974, 18, 2391-2397.
55. Loy, B. R., J. Polym. Sci. Polym. Chem. Ed., 1976, 14, 23
56. Vrijbergen, R. R., Soeteman, A. A. and Smit, J. A. M., J. Appl. Polym. Sci., 1978, 22, 1267-1276.
57. McCrackin, F. L., J. Appl. Polym. Sci., 1977, 21, 191-198.
58. Mahabadi, H. K. and O'Driscoll, K. F., J. Appl. Polym. Sci., 1977, 21, 1283-1287.
59. Weiss, A. R. and Cohn-Ginsberg, E. J. Polym. Sci., Part B, 1969, 7, 379-381.
60. Mori, S., Anal. Chem. 1981, 53, 1813-1818.
61. Chi Wu, Ju Zuo, and Ben Chu, Macromolecules, 1989, 22 (No.2), 633

62. Burchard, W., Schmidt, M. and Stockmayer, W. H., Macromolecules, 1980, 13, 1265.
63. Kajiwara, K. and Burchard, W., Polymer, 1981, 22, 1621.
64. Gordon, M., Proc. Roy. Soc. (London), 1962, 268, 240.
65. Flory, J., J. Am. Chem. Soc., 63, 1941, 1096, 3083, 3091.
66. Stockmayer, W. H., J. Chem. Phys., 12, 1944, 125.
67. de Gennes, P. G., Scaling Concepts in Polymer Physics, (Cornell Univ. Press, N.Y., 1979).
68. Stauffer, D., Coniglio, and Adam, M. Adv. Polym. Sci., 1982, 44, 103.
69. Ernst, M. H., Ziff, R. M. and Hendriks, E. M., J. Coll. Interface Sci., 1984, 97, 266.
70. Herrmann, H., Landau, D. P. and Stauffer, D., Phys. Rev. Lett., 1983, 49, 412.
71. Stauffer, D., Phys. Rep., 1979, 54, 1.
72. Leibler, L. and Schosseler, F., Phys. Rev. Lett., 1985, 55, 1110.
73. Fischer, R. F., J. Polym. Sci., 1960, 44, 155.
74. Smoluchowski, M. V., Physik. Z., 1916, 17, 585; Z. Phys. Chem., 1918, 92, 129.
75. Golovin, A. M., Bull. Akad. Sci. SSSR Geophy. Ser., (English Transl.), 1963, 482.
76. Scott, W. T., J. Atmos. Sci., 1968, 25, 54.
77. Scott, W.T., Analytic studies of cloud droplet coalescence. I. Tech. Rept., No. 9, Desert Research Institute, University of Nevada, 1965, 72.
78. Lu, B., J. of Statistical Physics, 1987, 49, Nos. 3/4, 669
79. Dusek, K., Lunak, S., Matejke, L., Polymer Bulletin, 1982, 7, 145.
80. Chu, B. and Wu, C., Macromolecules, 1988, 21, 1729.
81. Wu C., Zuo, J. and Chu, B., Macromolecules, 1989, 22 (No. 2), 838
82. Wu C., Chu, B. and Stell, G., submitted to J. of Chem. Phys. for publication.

TABLE I

Properties of Epoxy Polymer (1,4-butanediol diglycidyl ether with cis-1,2-cyclohexanedicarboxylic anhydride) during the Curing Process

| Sample # | Conversion (% CH) | $M_w$ (g/mol)      |                    | $\langle R_g^2 \rangle^{1/2}$ (Å) |     | $A_2$ ( $\frac{ml}{g^2} mol$ ) |                       |
|----------|-------------------|--------------------|--------------------|-----------------------------------|-----|--------------------------------|-----------------------|
|          |                   | X-ray              | LLS                | X-ray                             | LLS | X-ray                          | LLS                   |
| 1        | 6.5%              | $4.32 \times 10^3$ | $4.11 \times 10^3$ | 29                                | -   | -                              | $1.45 \times 10^{-3}$ |
| 2        | 13.3%             | $6.14 \times 10^3$ | $6.07 \times 10^3$ | 36                                | -   | -                              | $1.26 \times 10^{-3}$ |
| 3        | 20.0%             | $8.23 \times 10^3$ | $8.23 \times 10^3$ | 44                                | -   | $1.05 \times 10^{-3}$          | $1.01 \times 10^{-3}$ |
| 4        | 26.5%             | $1.25 \times 10^4$ | $1.22 \times 10^4$ | 55                                | -   | -                              | $8.70 \times 10^{-4}$ |
| 5        | 33.5%             | $2.11 \times 10^4$ | $2.04 \times 10^4$ | 70                                | -   | -                              | $7.41 \times 10^{-4}$ |
| 6        | 36.0%             | $3.37 \times 10^4$ | $3.15 \times 10^4$ | 85                                | -   | $6.12 \times 10^{-4}$          | $6.30 \times 10^{-4}$ |
| 7        | 38.5%             | $5.60 \times 10^4$ | $5.00 \times 10^4$ | 112                               | 105 | -                              | $5.25 \times 10^{-4}$ |
| 8        | 40.0%             | -                  | $7.68 \times 10^4$ | -                                 | 128 | -                              | $4.57 \times 10^{-4}$ |
| 9        | 41.0%             | -                  | $1.03 \times 10^5$ | -                                 | 150 | -                              | $4.17 \times 10^{-4}$ |
| 10       | 42.5%             | -                  | $1.42 \times 10^5$ | -                                 | 191 | -                              | $3.63 \times 10^{-4}$ |
| 11       | 44.0%             | -                  | $2.19 \times 10^5$ | -                                 | 222 | -                              | $3.16 \times 10^{-4}$ |
| 12       | 45.3%             | -                  | $3.01 \times 10^5$ | -                                 | 257 | -                              | $2.88 \times 10^{-4}$ |
| 13       | 46.5%             | -                  | $4.97 \times 10^5$ | -                                 | 314 | -                              | $2.51 \times 10^{-4}$ |

Table II

(a) Fractal dimension  $d_f$  of epoxy polymer solutions based on  $I(K) \sim K^{d_f}$  of Eq. (6) with  $(2/R_g) < K < Y$

| Sample | $Y^{-1}(\text{Å}) = 30$ | $d_f$     |           |           |
|--------|-------------------------|-----------|-----------|-----------|
|        |                         | 20        | 15        | 10        |
| 13     | 2.17±0.01               | 2.16±0.01 | 2.14±0.02 | 2.10±0.03 |
| 12     | 2.17±0.01               | 2.17±0.02 | 2.13±0.03 | 2.11±0.04 |
| 11     | 2.18±0.02               | 2.17±0.02 | 2.14±0.02 | 2.12±0.03 |
| 10     | 2.18±0.01               | 2.17±0.01 | 2.15±0.02 | 2.12±0.02 |
| 9      | 2.17±0.02               | 2.17±0.02 | 2.14±0.03 | 2.10±0.03 |
| 8      | 2.17±0.05               | 2.16±0.03 | 2.13±0.03 | 2.10±0.04 |
| 7      | 2.18±0.05               | 2.17±0.04 | 2.14±0.04 | 2.11±0.05 |
| 6      | 2.16±0.05               | 2.17±0.04 | 2.13±0.04 | 2.09±0.05 |
| 5      | 2.15±0.07               | 2.16±0.05 | 2.13±0.04 | 2.10±0.05 |
| 4      | -                       | 2.12±0.06 | 2.10±0.05 | 2.05±0.06 |
| 3      | -                       | 2.05±0.08 | 2.00±0.06 | 1.94±0.06 |
| 2      | -                       | -         | 2.04±0.08 | 1.96±0.07 |
| 1      | -                       | -         | -         | 1.90±0.08 |

Table II

(b) Coil behavior of epoxy polymers between the mesh points based on  $I(K) \sim K^{-\beta}$  with  $Y < K < (1/4) \text{ \AA}^{-1}$

| Sample | $Y^{-1}(\text{\AA}) = 30$ | $\beta$   |           |           |
|--------|---------------------------|-----------|-----------|-----------|
|        |                           | 20        | 15        | 10        |
| 13     | 1.74±0.06                 | 1.67±0.05 | 1.64±0.06 | 1.59±0.09 |
| 12     | 1.76±0.05                 | 1.69±0.05 | 1.65±0.07 | 1.61±0.09 |
| 11     | 1.75±0.06                 | 1.67±0.05 | 1.63±0.07 | 1.60±0.09 |
| 10     | 1.74±0.05                 | 1.68±0.06 | 1.67±0.07 | 1.65±0.10 |
| 9      | 1.73±0.06                 | 1.67±0.05 | 1.65±0.07 | 1.62±0.10 |
| 8      | 1.74±0.06                 | 1.68±0.06 | 1.66±0.07 | 1.63±0.10 |
| 7      | 1.72±0.07                 | 1.67±0.06 | 1.65±0.07 | 1.62±0.09 |
| 6      | 1.71±0.07                 | 1.68±0.06 | 1.66±0.05 | 1.62±0.10 |
| 5      | 1.70±0.06                 | 1.68±0.06 | 1.65±0.06 | 1.61±0.10 |
| 4      | 1.68±0.07                 | 1.67±0.07 | 1.65±0.07 | 1.60±0.10 |
| 3      | 1.68±0.06                 | 1.67±0.07 | 1.64±0.06 | 1.58±0.11 |
| 2      | 1.67±0.08                 | 1.68±0.07 | 1.66±0.07 | 1.59±0.10 |
| 1      | 1.65±0.08                 | 1.67±0.07 | 1.66±0.07 | 1.59±0.11 |

Table III

Determination of  $\xi$  based on plots of  $\log (W_{\text{mea}}/W_{\text{cal}})$  versus  $\log K$ .<sup>a</sup>

| Sample    | 3 <sup>b</sup> | 4 <sup>b</sup> | 5            | 6            | 7            | 8            | 9            | 10           | 11           | 12           | 13           |
|-----------|----------------|----------------|--------------|--------------|--------------|--------------|--------------|--------------|--------------|--------------|--------------|
| $\xi$ (Å) | 18.4<br>±4.7   | 18.5<br>±4.8   | 18.9<br>±3.9 | 20.3<br>±3.7 | 19.2<br>±3.0 | 20.1<br>±3.4 | 18.9<br>±4.2 | 19.5<br>±3.3 | 20.0<br>±3.5 | 20.4<br>±3.4 | 19.7<br>±3.0 |

<sup>a</sup>  $\xi^{-1}$  is determined by the intercept between  $W_{\text{mea}}/W_{\text{cal}} = 1$  and the straight line with slope  $\sim 0.49$ .      <sup>b</sup> Estimated value

TABLE IV.

Experimental results based on the MSVD method for the epoxy polymer samples in MEK at 25°C and  $\lambda_0 = 488$  nm.

| Sample | conversion<br>(CH%) | $M_w$ (g/mol)      | $\bar{D}_O^0$ (cm <sup>2</sup> /sec) | $\mu_2/\bar{\Gamma}^2$ | f    | $k_d$ (mL/g) |
|--------|---------------------|--------------------|--------------------------------------|------------------------|------|--------------|
| 1      | 6.5                 | $4.32 \times 10^3$ | $2.71 \times 10^{-6}$                | 0.63                   | -    | 0            |
| 2      | 13.3                | $6.14 \times 10^3$ | $2.27 \times 10^{-6}$                | 0.61                   | -    | 11           |
| 3      | 20.0                | $8.23 \times 10^3$ | $1.77 \times 10^{-6}$                | 0.56                   | -    | 16           |
| 4      | 26.5                | $1.25 \times 10^4$ | $1.29 \times 10^{-6}$                | 0.53                   | -    | 22           |
| 5      | 33.5                | $2.11 \times 10^4$ | $1.00 \times 10^{-6}$                | 0.51                   | -    | 29           |
| 6      | 36.0                | $3.37 \times 10^4$ | $7.98 \times 10^{-7}$                | 0.48                   | -    | 36           |
| 7      | 38.5                | $5.00 \times 10^4$ | $6.45 \times 10^{-7}$                | 0.47                   | 0.15 | 48           |
| 8      | 40.0                | $7.68 \times 10^4$ | $5.26 \times 10^{-7}$                | 0.46                   | 0.17 | 63           |
| 9      | 41.0                | $1.03 \times 10^5$ | $4.38 \times 10^{-7}$                | 0.45                   | 0.13 | 79           |
| 10     | 42.5                | $1.42 \times 10^5$ | $3.68 \times 10^{-7}$                | 0.43                   | 0.18 | 89           |
| 11     | 44.0                | $2.19 \times 10^5$ | $2.97 \times 10^{-7}$                | 0.40                   | 0.21 | 101          |
| 12     | 45.3                | $3.01 \times 10^5$ | $2.60 \times 10^{-7}$                | 0.42                   | 0.16 | 132          |
| 13     | 46.5                | $4.97 \times 10^5$ | $2.05 \times 10^{-7}$                | 0.40                   | 0.19 | 141          |